



## The influence of winter water on phytoplankton blooms in the Chukchi Sea



Kate E. Lowry<sup>a,\*</sup>, Robert S. Pickart<sup>b</sup>, Matthew M. Mills<sup>a</sup>, Zachary W. Brown<sup>a</sup>,  
Gert L. van Dijken<sup>a</sup>, Nicholas R. Bates<sup>c</sup>, Kevin R. Arrigo<sup>a</sup>

<sup>a</sup> Department of Earth System Science, Stanford University, Stanford, CA 94305, USA

<sup>b</sup> Woods Hole Oceanographic Institution, Woods Hole, MA 02540, USA

<sup>c</sup> Bermuda Institute of Ocean Sciences, St. Georges, Bermuda

### ARTICLE INFO

Available online 11 June 2015

#### Keywords:

Phytoplankton  
Winter water  
Under-ice blooms  
Biological hotspots  
Chukchi Sea

### ABSTRACT

The flow of nutrient-rich winter water (WW) through the Chukchi Sea plays an important and previously uncharacterized role in sustaining summer phytoplankton blooms. Using hydrographic and biogeochemical data collected as part of the ICESCAPE program (June–July 2010–11), we examined phytoplankton bloom dynamics in relation to the distribution and circulation of WW (defined as water with potential temperature  $\leq -1.6$  °C) across the Chukchi shelf. Characterized by high concentrations of nitrate (mean:  $12.3 \pm 5.13$   $\mu\text{mol L}^{-1}$ ) that typically limits primary production in this region, WW was correlated with extremely high phytoplankton biomass, with mean chlorophyll *a* concentrations that were 3-fold higher in WW ( $8.64 \pm 9.75$   $\mu\text{g L}^{-1}$ ) than in adjacent warmer water ( $2.79 \pm 5.58$   $\mu\text{g L}^{-1}$ ). Maximum chlorophyll *a* concentrations ( $\sim 30$   $\mu\text{g L}^{-1}$ ) were typically positioned at the interface between nutrient-rich WW and shallower, warmer water with more light availability. Comparing satellite-based calculations of open water duration to phytoplankton biomass, nutrient concentrations, and oxygen saturation revealed widespread evidence of under-ice blooms prior to our sampling, with biogeochemical properties indicating that blooms had already terminated in many places where WW was no longer present. Our results suggest that summer phytoplankton blooms are sustained for a longer duration along the pathways of nutrient-rich WW and that biological hotspots in this region (e.g. the mouth of Barrow Canyon) are largely driven by the flow and confluence of these extremely productive pathways of WW that flow across the Chukchi shelf.

© 2015 Elsevier Ltd. All rights reserved.

### 1. Introduction

Located north of the Bering Strait between Alaska and Far East Russia, the Chukchi Sea is the gateway of the Pacific Ocean to the Arctic. With a total area of 620,000 km<sup>2</sup> and a median depth of approximately 50 m (Jakobsson, 2002), the Chukchi Sea contains a wide and shallow continental shelf that comprises 10% of the total Arctic Ocean shelf area (Jakobsson et al., 2004; Carmack and Wassmann, 2006). The importance of the Chukchi Sea as an inflow shelf sea (Carmack and Wassmann, 2006) that ventilates the upper halocline of the Arctic Ocean (Woodgate and Aagaard, 2005b; Woodgate et al., 2005a) motivates a thorough understanding of the physical and biogeochemical processes that modify Pacific-origin water masses as they transit the shelf en route to the basin.

The Chukchi Sea is a region of intense summer biological

activity with a rich benthic community that supports abundant populations of marine mammals and seabirds (Loeng et al., 2005; Dunton et al., 2005; Grebmeier et al., 2006). In recent decades, the Arctic Ocean has experienced unprecedented reductions in sea ice cover and thickness (Kwok and Rothrock, 2009; Serreze et al., 2007; Stroeve et al., 2011), accompanied by an increased heat and freshwater flux through the Bering Strait (Woodgate et al., 2012). The impacts of these changes on the global carbon cycle (Bates et al., 2011) and the marine ecosystem of the Chukchi Sea (Grebmeier, 2012) are only beginning to be understood. Of particular interest is how the primary producers that form the base of the food web are being affected by the pronounced changes in the physical environment. Previous work suggests that phytoplankton are already responding to reduced sea ice cover and thickness, with evidence for increased primary production in open water (Arrigo and Van Dijken, 2011) and beneath the thinning sea ice cover (Arrigo et al., 2012, 2014; Palmer et al., 2014, 2013; Lowry et al., 2014). To fully comprehend the significance of these changes, it is necessary to further our understanding of bloom

\* Corresponding author. Tel.: +1 650 736 0688.

E-mail address: [lowryk@stanford.edu](mailto:lowryk@stanford.edu) (K.E. Lowry).

dynamics in this region.

Pacific-origin water flows northward through the Bering Strait due to the sea surface height differential resulting from the salinity difference between the Arctic and Pacific Oceans (Coachman et al., 1975). Upon entering the Chukchi Sea, the flow is steered primarily by shelf bathymetry into three branches, which to some degree are distinguished by water mass properties set within the Bering Sea (Coachman et al., 1975; Overland and Roach, 1987; Weingartner et al., 2005). Differences in temperature, salinity ( $S$ ), and nutrient concentrations between these pathways result in significant variations in biogeochemical properties across the shelf (Walsh et al., 1989; Cooper et al., 1997; Codispoti et al., 2005, 2013). In summertime, the easternmost pathway advects Alaskan Coastal Water, which is relatively warm ( $> 2\text{ }^{\circ}\text{C}$ ), fresh ( $S < 32$ ), and nutrient-poor (pre-bloom  $\text{NO}_3^- < 10\text{ }\mu\text{mol L}^{-1}$ ) due to the input of river runoff and the biological utilization of nutrients in the eastern Bering Sea. The middle flow branch, which progresses through the Central Channel between Hanna and Herald Shoals, consists largely of colder and saltier Bering Shelf Water (BSW) with moderate nutrient concentrations (pre-bloom  $\text{NO}_3^- > 10\text{ }\mu\text{mol L}^{-1}$ ). The westernmost branch follows Hope Valley into Herald Canyon and transports a large amount of Anadyr Water (AW), which is the saltiest of the three Chukchi Sea water masses and has the highest nutrient concentration (pre-bloom  $\text{NO}_3^- > 15\text{ }\mu\text{mol L}^{-1}$ ), owing to the upwelling of nutrient-rich waters in the Northern Bering Sea (Hansell et al., 1993; Lee et al., 2007). The precise division of transport between the branches is currently unknown. Using relatively sparse mooring data, Woodgate et al. (2005b) estimated a roughly even split between the branches, but recent shipboard surveys suggest that, in summer, the majority of the flow is contained in the two eastern branches (Gong and Pickart, 2015; Itoh et al., 2015).

The water mass properties in the Chukchi Sea are heavily influenced by the seasonal cycle of sea ice, both locally on the Chukchi shelf and to the south in the Bering Sea. In the winter, sea ice formation causes brine rejection that can mix the entire water column and cool it to the freezing point (approximately  $-1.9\text{ }^{\circ}\text{C}$ ) (e.g. Woodgate et al., 2005b). When the convection reaches the bottom it suspends regenerated nutrients from the sediments into the water column. The resulting water mass, known as winter water (WW), is cold, dense, and high in nutrients. The water so formed in the Bering Sea flows northward through Bering Strait during the winter months and into the spring (Woodgate et al., 2005b). However, the occurrence of leads and polynyas on the Chukchi shelf during the winter can lead to further re-freezing and the formation of “hyper-saline” WW (Weingartner et al., 1998; Itoh et al., 2012).

Although there are few winter and spring measurements in the Chukchi Sea, modeling results (Zhang et al., 2010) and field studies (e.g. Codispoti et al., 2005) indicate that surface waters are nutrient-replete in the Chukchi Sea, with  $\text{NO}_3^-$  concentrations as high as  $10\text{--}20\text{ }\mu\text{mol L}^{-1}$  in non-coastal shelf waters. As sea ice retreats in the summer, the water column becomes re-stratified as surface waters freshen and warm due to a combination of ice melt, solar heating, and the influx of Pacific summer waters from the Bering Sea (Woodgate and Aagaard, 2005a; Gong and Pickart, 2015). The WW remaining on the Chukchi shelf is gradually modified by mixing with these waters and/or by direct solar heating (Weingartner et al., 2005; Gong and Pickart, 2012). As a result, the presence of WW on the shelf in summer is spatially variable, with residence times determined by the bathymetry and circulation of the Chukchi Sea (Pickart et al., submitted for publication). By the end of summer, all of the WW gets flushed from the shelf, largely through Herald Canyon in the west (Pickart et al., 2010) and Barrow Canyon in the east (Pickart et al., 2005; Woodgate et al., 2005b; Itoh et al., 2015).

The high nutrient content and persistence of WW on the

Chukchi shelf through the spring and summer suggests that this water mass plays an important, yet previously uncharacterized, role in influencing phytoplankton blooms. In this study, we examine the relationship between the early-summer hydrographic conditions in the Chukchi Sea and the phytoplankton blooms that occur on the shelf, with specific focus on the role of the nutrient-rich WW in initiating and sustaining phytoplankton blooms both before and after sea ice retreat. We assess the biological significance of WW in the summer as it drains across the Chukchi shelf by relating the location of WW to biogeochemical properties such as phytoplankton biomass, oxygen ( $\text{O}_2$ ) saturation, and concentrations of nutrients and dissolved inorganic carbon (DIC). To fully elucidate the relationship between WW and phytoplankton blooms in this seasonally ice-free ecosystem, we incorporate field results from both under the sea ice and in open water, and use satellite imagery of sea ice to provide further environmental context.

## 2. Methods

### 2.1. Study region

As part of the NASA-funded Impacts of Climate on EcoSystems and Chemistry of the Arctic Pacific Environment (ICESCAPE) program, two field campaigns were carried out in the Chukchi Sea aboard USCGC Healy, from 18 June to 16 July 2010 (HLY1001) and from 28 June to 24 July 2011 (HLY1101). The present analysis focuses on the continental shelf of the northeastern Chukchi Sea, using data from seven transects that together span the shallow shelf waters of this region (Fig. 1). Six of the seven transects considered here were occupied in 2011, while the southernmost transect (the Central Channel line) was sampled in 2010. The Chukchi North and Hanna Shoal North transects were occupied on both cruises, providing an opportunity to compare hydrographic conditions between 2010 and 2011. Except where otherwise noted, data presented for these two transects were collected in 2011 when the sampling was more comprehensive.

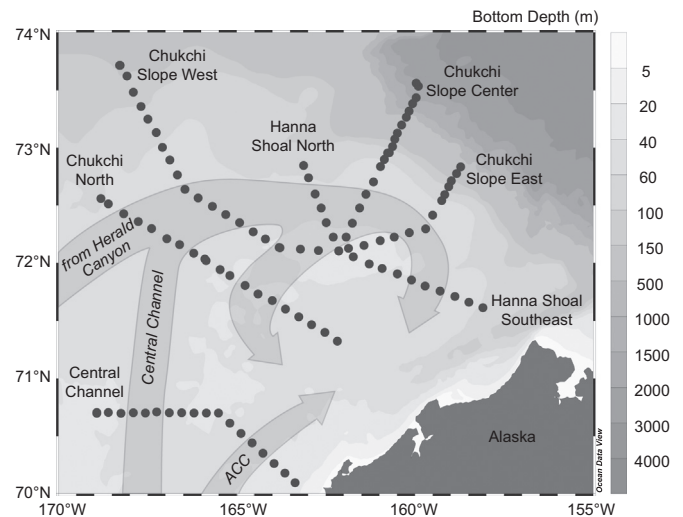


**Fig. 1.** Map of the northeastern Chukchi Sea illustrating bathymetry, the seven transects sampled as part of our field campaign in 2010–2011 that we focus on in this study, and the main pathway of winter water (WW) as it flowed across the Chukchi shelf during our sampling period (as identified and described in more detail by Pickart et al. (submitted for publication)).

## 2.2. Field methods and laboratory analysis

### 2.2.1. Shipboard sampling

Vertical profiles of temperature, salinity, dissolved O<sub>2</sub>, fluorescence, and photosynthetically active radiation (PAR) were obtained approximately every 15 km using a Sea-Bird 911+ conductivity-temperature-depth instrument (CTD) with an SBE43 O<sub>2</sub> sensor (Sea-Bird Electronics), a fluorometer (AQIII, Chelsea Technologies Group, Ltd.), and a PAR sensor (QSP2300, Biospherical Instruments, Inc.). The CTD system was mounted on a rosette with twelve 30-liter Niskin bottles. Water samples were collected at a set of standard depths (5, 10, 25, 50, 75, 100, 150, and 200 m), and also at the depth of the fluorescence maximum and near the bottom (typically within 2–5 m of the seafloor). Most of the stations were occupied on the shelf and hence were shallower than 60 m. The temperature and conductivity sensors were calibrated pre- and post-cruise at Sea-Bird Electronics, and the conductivity sensor was also calibrated during the cruise using the deepest water sample salinity data. Based on this information, the estimated accuracies are 0.008 °C for temperature and 0.004 for salinity on the shelf, and 0.002 °C and 0.002, respectively, in deeper water.

Water samples were taken for O<sub>2</sub> concentration using standard Winkler titrations for sensor calibration and for a suite of biogeochemical properties, including nutrients, dissolved inorganic carbon (DIC), chlorophyll *a* (Chl *a*), and particulate organic carbon (POC). Methods for these analyses are briefly presented below, with additional detail provided by Arrigo et al. (2014).

Currents were measured on both cruises using the Healy's hull-mounted Ocean Surveyor 150 KHz acoustic Doppler current profiler (ADCP). The data were acquired using the UHDAS software package from the University of Hawaii, with additional processing done using the CODAS3 software utility (<http://currents.soest.hawaii.edu>). Following this, the barotropic tidal signal was removed from each profile using the Oregon State University model (<http://volkov.oce.orst.edu/tides>; Padman and Erofeeva, 2004). The uncertainty of the final product is estimated to be  $\pm 2 \text{ cm s}^{-1}$ .

### 2.2.2. Nutrients and dissolved inorganic carbon

Discrete water column samples were analyzed for nutrients on board the ship with a Seal Analytical continuous-flow Auto-Analyzer 3 using a modification of the method of Armstrong et al. (1967). In this study, we focus primarily on nitrate (NO<sub>3</sub><sup>-</sup>), but also consider concentrations of silicate (Si(OH)<sub>4</sub>) and phosphate (PO<sub>4</sub><sup>3-</sup>). Seawater samples for DIC were collected at each station into pre-cleaned ~300 mL borosilicate bottles, poisoned with HgCl<sub>2</sub> to halt biological activity, and then sealed after the cast. The analysis was done post-cruise at the Bermuda Institute of Ocean Sciences (BIOS) using a highly precise (~0.025%; < 0.5 mmol kg<sup>-1</sup>) gas extraction/coulometric detection system (Bates et al., 2005), along with Certified Reference Materials (provided by A. G. Dickson, Scripps Institution of Oceanography). The resulting accuracy was 0.05% (~0.5 mmol kg<sup>-1</sup>).

### 2.2.3. Phytoplankton

Samples for Chl *a* were filtered onto 25 mm Whatman GF/F filters (nominal pore size 0.7 μm), placed in 5 mL of 90% acetone, and then extracted in the dark at 3 °C for 24 h. Chl *a* was measured fluorometrically (Holm-Hansen et al., 1965) on-board using a Turner 10-AU fluorometer (Turner Designs, Inc.) calibrated with pure Chl *a* (Sigma). POC samples were collected by filtering water samples onto pre-combusted (450 °C for 4 h) 25 mm Whatman GF/F filters. Filter blanks were produced by passing ~50 mL of 0.2 μm filtered seawater through a GF/F. All filters were then immediately dried at 60 °C and stored dry until analysis. Prior to

analysis, samples and blanks were fumed with concentrated HCl, dried at 60 °C, and packed into tin capsules (Costech Analytical Technologies, Inc.) for elemental analysis on an Elementar Vario EL Cube (Elementar Analysensysteme GmbH, Hanau, Germany) interfaced to a PDZ Europa 20–20 isotope ratio mass spectrometer (Sercon Ltd., Cheshire, UK). Standards included peach leaves and glutamic acid.

At select stations, we also determined the maximum efficiency of photosystem II (Fv:Fm) from discrete water column samples by fast repetition rate fluorometry (FRRf) (Kolber et al., 1998), with excitation at 470 nm. These samples were collected, dark acclimated for ~30 min at in situ temperatures, and measured on the FRRf within one hour of collection. Blanks for individual samples analyzed by FRRf were prepared by gentle filtration through a 0.2 μm polycarbonate syringe filter before measurement using identical protocols. All Fv:Fm values were corrected for blank effects (Cullen and Davis, 2003).

## 2.3. Classification of winter water

Consistent with several companion studies (Pickart et al., submitted for publication; Brown et al., 2015-a; Mills et al., 2015), WW is defined here as the water with potential temperature ( $\theta$ ) below  $-1.6$  °C. This distinguishes the most recently ventilated, and therefore most pure, WW from the modified (via solar heating and/or mixing with summer water masses) 'remnant' WW ( $-1.6$  °C <  $\theta$  <  $-1$  °C) also found on the Chukchi shelf in the summer (Gong and Pickart, 2015). We note that related studies (e.g. Brown et al., 2015-a; Mills et al., 2015; Strong et al., in preparation) exclude waters with relatively low NO<sub>3</sub><sup>-</sup> (< 10 μmol L<sup>-1</sup>) from the definition of WW to avoid misidentifying cold, near-surface sea ice melt water. However, in the seven transects of this study, all near-surface (< 10 m) water samples colder than  $-1.6$  °C were characterized by salinities greater than 31.5 and were part of a continuous water mass that extended from depth to the surface. For this reason, we include all samples meeting the temperature requirement ( $\theta \leq -1.6$  °C) in our definition of WW, regardless of nutrient content.

## 2.4. Hydrographic analysis

Vertical sections of water column variables were constructed using either the DIVA gridding package in Ocean Data View 4 (Schlitzer, 2014) or a Laplacian-spline interpolator (see Pickart et al., 2013). We consider sections of  $\theta$ , salinity, absolute geostrophic velocity, NO<sub>3</sub><sup>-</sup>, DIC, Chl *a*, POC, and O<sub>2</sub> saturation (calculated in Ocean Data View 4), focusing on the upper 60 m of the water column. The absolute geostrophic velocity was calculated by referencing the gridded thermal wind shear to the gridded cross-transect ADCP velocity for each grid pair across the section. To illustrate stratification and mixing processes and the location of WW in relation to our biogeochemical measurements, the hydrographic sections are overlain by contours of potential density ( $\sigma_\theta$ ; kg m<sup>-3</sup>, thin lines) and the delimiting WW isotherm ( $\theta = -1.6$  °C, thick line). For stations with bottom depths shallower than 60 m, the seafloor is indicated by a dark gray color on the hydrographic section plots and the vertical region between the deepest sample and the seafloor is illustrated in light gray. The statistical significance of differences between WW and non-WW samples for each transect were assessed through a series of *t*-tests following log transformation of the data.

## 2.5. Open water duration

Annual cycles of sea ice concentration for 2010 and 2011 were obtained at each station from daily AMSR-E (Advanced Microwave

Scanning Radiometer – Earth Observing System) satellite images at 12.5 km resolution, accessed from the National Snow and Ice Data Center (NSIDC). The sea ice concentrations at each station were then used to calculate open water duration, defined as the

number of days that the station location had < 50% ice concentration between the date of initial ice retreat and the sampling date. In cases where ice retreated and re-advanced over a particular location before the final retreat (due to wind shifts, for

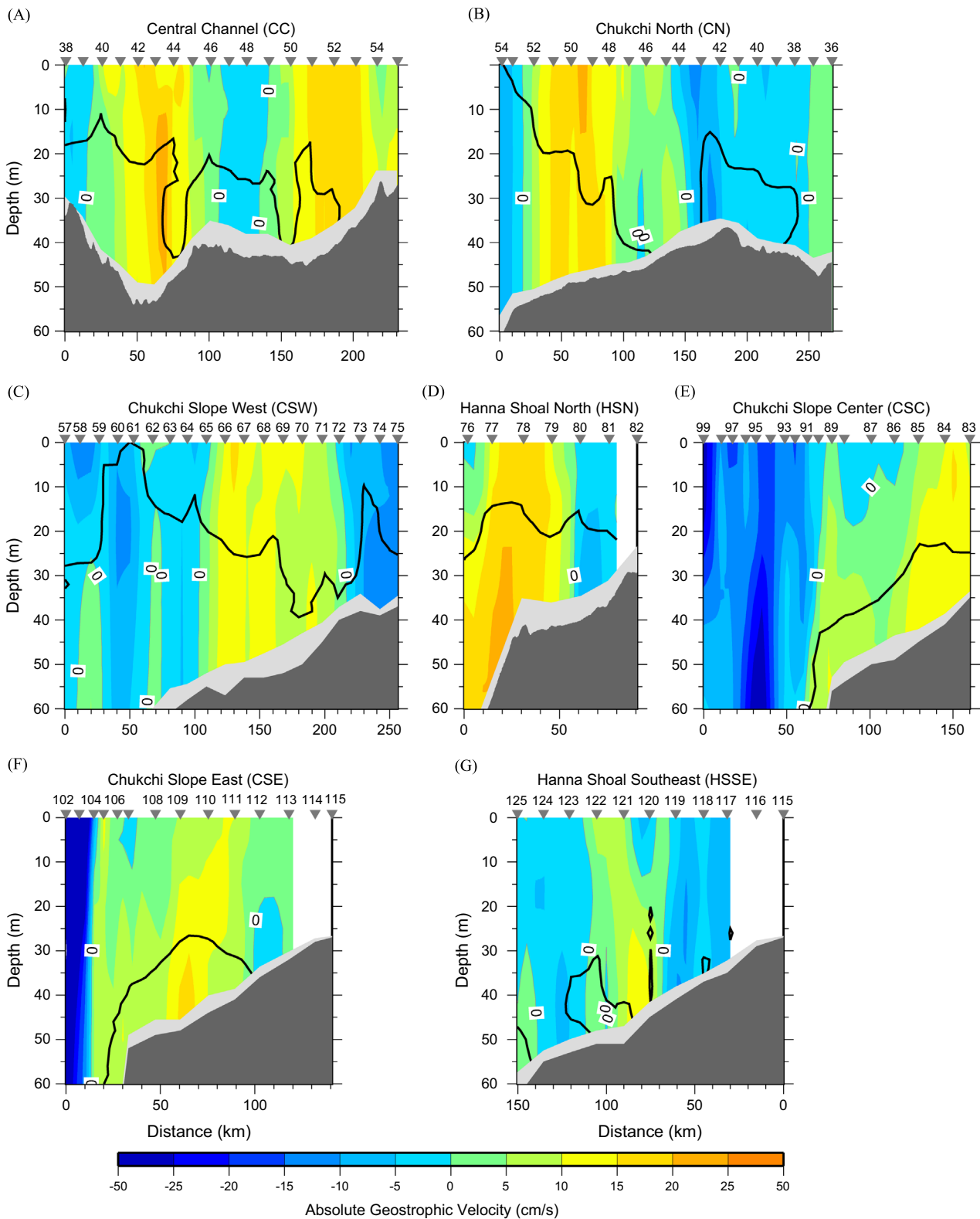


**Fig. 2.** Vertical sections of absolute geostrophic velocity illustrating the speed and direction of currents through transects (A) Central Channel, (B) Chukchi North, (C) Chukchi Slope West, (D) Hanna Shoal North, (E) Chukchi Slope Center, (F) Chukchi Slope East, and (G) Hanna Shoal Southeast. Positive values indicate flow into the page, while negative values indicate flow out of the page. Locations where absolute geostrophic velocity equals zero are labeled and sections are overlain by the WW isotherm ( $\theta = -1.6^\circ\text{C}$ ; black line).

example), we did not include those periods with > 50% concentration. Calculated in this way, open water duration is a proxy for the amount of time that phytoplankton at a given station were exposed to the full incident sunlight of the open water environment, as opposed to the lower light conditions present underneath

sea ice. For a detailed justification of the 50% ice concentration threshold used to distinguish open water from ice cover in this region, see [Lowry et al. \(2014\)](#). Plots of open water duration are presented along with the hydrographic sections to provide environmental context for each transect.

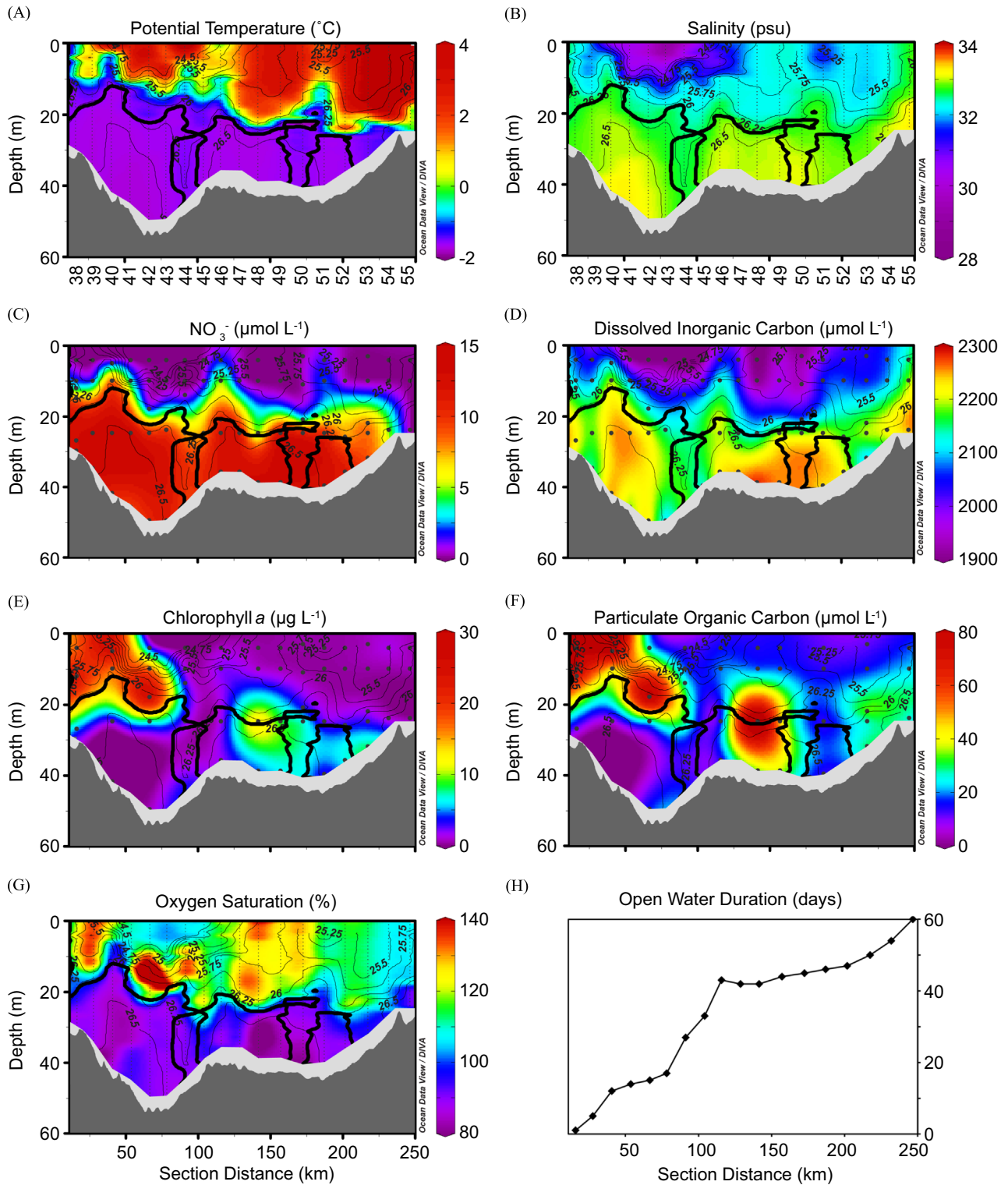


**Fig. 3.** The Central Channel transect was sampled on 29 June–1 July 2010 and is displayed here from northwest (left) to southeast (right). (A–G) Hydrographic sections of (A)  $\theta$ , (B) salinity, (C)  $\text{NO}_3^-$ , (D) DIC, (E) Chl *a*, (F) POC, and (G)  $\text{O}_2$  saturation, overlain by  $\sigma_{\theta}$  ( $\text{kg m}^{-3}$ ; thin black lines with labels) and the WW isotherm ( $\theta = -1.6^{\circ}\text{C}$ ; thick black line). Station numbers are below (A) and (B) and black dots represent sampling depths. (H) Satellite-based open water duration, indicating the number of days each station was in open water from the time of ice retreat until the date of sampling. Note that this transect is referred to as the Central Shelf transect in [Gong and Pickart \(2015\)](#).

### 3. Results

#### 3.1. Presence and flow of WW

For the seven transects considered in this study, WW was found at 78% (82 of 105) of the stations, demonstrating the prevalence of this water mass laterally throughout our study region. However, WW was observed at only 35% (1678 of 4833) of the one-meter CTD bins in the upper 60 m, a consequence of the non-uniform vertical distribution of WW. WW was frequently observed at depth but was found much less commonly near the surface during our summer sampling period. The salinity range of the WW was relatively wide (31.23–33.38) and overlapped with the salinity range of nearby warmer water.

The flow pathways of WW across the Chukchi shelf observed during the ICESCAPE program were identified and mapped by Pickart et al. (submitted for publication). The main pathways are included in Fig. 1. Much of the WW on the northeast shelf drains through Barrow Canyon (e.g. Pickart et al., 2005; Weingartner et al., 2005). However, as described by Pickart et al. (submitted for publication), the precise flow paths leading to the canyon are more complex than previously thought. As seen in Fig. 1, a branch of WW enters our study area from the west, presumably emanating from the western-most branch (Pickart et al., 2010), and joins the Central Channel WW pathway. As this combined flow encounters Hanna Shoal it bifurcates, with a portion circulating cyclonically around the shoal and the rest being diverted southward. The southward limb is then believed to turn eastward to join the coastal branch of WW before flowing into Barrow Canyon en route to the Arctic Basin.

#### 3.2. Vertical sections

Next, we relate the location and nature of the flow of WW through each transect to the various physical and biogeochemical properties, using vertical sections of salinity, nutrients, DIC, phytoplankton biomass, and O<sub>2</sub> saturation, as well as plots of satellite-derived open water duration. We begin our description with the southernmost transect and then follow the pathway of WW around the northern side of Hanna Shoal (Fig. 1).

##### 3.2.1. Central Channel

The southernmost transect extended west to east across Central Channel to the vicinity of the Alaskan coast (from left to right; Figs. 1, 2A, and 3). Potential temperature along the Central Channel

transect (Fig. 3A) revealed that WW was present at three distinct locations (the thick black contour in the vertical sections marks the  $-1.6$  °C isotherm, which is the upper limit of WW). The absolute geostrophic velocity (Fig. 2A) indicated that the largest volume of WW (located to the west) was flowing to the north within the Central Channel pathway (Fig. 1) at speeds as fast as  $15\text{--}20$  cm s<sup>-1</sup>. A smaller volume of WW was progressing southward at a relatively slow speed ( $\leq 5$  cm s<sup>-1</sup>), likely due to a small recirculation from the main pathway (Figs. 1 and 2A; see also Pickart et al., submitted for publication). The smallest pathway of WW (located to the east) was also flowing northward, advected by the Alaskan Coastal Current at speeds ranging from 15 to 20 cm s<sup>-1</sup>.

The temperature of WW generally decreased with depth. The salinity range of WW in the Central Channel transect was 32.40–33.25 (Fig. 3B). The highest salinity WW was located in the Central Channel pathway, while fresher WW was advected by the Alaskan Coastal Current. Note that a small amount of high salinity water ( $\sim 33.30$ ) was also found in warmer ( $\sim 0$  °C) bottom waters near the coast of Alaska (St. 55; Fig. 3B), indicating that WW was not always the highest salinity water mass on the Chukchi shelf. The mean potential density of the WW ( $\sigma_\theta = 26.46 \pm 0.13$  kg m<sup>-3</sup>) was significantly higher ( $p < 0.001$ ) than that of the non-WW ( $\sigma_\theta = 25.70 \pm 0.63$  kg m<sup>-3</sup>), a pattern that was generally true of all seven transects (Table 1).

WW was rich in dissolved nutrients, with all three pathways containing higher concentrations of NO<sub>3</sub><sup>-</sup> (Fig. 3C), silicate (not shown), and phosphate (not shown) than the adjacent warmer water. Nutrients were highest at the westernmost stations within the Central Channel WW pathway (Figs. 1 and 3C), with a maximum NO<sub>3</sub><sup>-</sup> concentration of  $14.7$  μmol L<sup>-1</sup>, and lowest at the easternmost stations within the Alaskan Coastal Current, with a maximum NO<sub>3</sub><sup>-</sup> concentration of  $11.9$  μmol L<sup>-1</sup>. The mean WW NO<sub>3</sub><sup>-</sup> concentration for all of the stations along the transect ( $12.0 \pm 1.71$  μmol L<sup>-1</sup>) was nearly 6.5-fold higher ( $p < 0.001$ ) than that of the non-WW ( $1.85 \pm 3.15$  μmol L<sup>-1</sup>; Table 1). Notably, the Central Channel transect had the highest non-WW mean NO<sub>3</sub><sup>-</sup> concentration of all seven transects (Table 1;  $p < 0.01$ ), due to the substantial presence of remnant WW ( $-1.6$  °C  $< \theta < -1$  °C) that was elevated in NO<sub>3</sub><sup>-</sup> (Fig. 3A and C). Concentrations of DIC (Fig. 3D) were also elevated along the WW pathways. On average, WW DIC concentrations in this transect were  $155$  μmol L<sup>-1</sup> higher than that of non-WW, with a mean value of  $2203 \pm 52$  μmol L<sup>-1</sup> for WW and  $2048 \pm 101$  μmol L<sup>-1</sup> for non-WW (Table 1;  $p < 0.001$ ). The vertical sections of both NO<sub>3</sub><sup>-</sup> and DIC show evidence of substantial

**Table 1**  
Mean and standard deviation of  $\theta$ , salinity,  $\sigma_\theta$ , NO<sub>3</sub><sup>-</sup>, DIC, Chl *a*, POC, and O<sub>2</sub> saturation for all WW ( $\theta \leq -1.6$  °C) and non-WW ( $\theta > -1.6$  °C) samples in the upper 60 m of each transect. Bold WW values indicate statistically significant differences from the respective non-WW values ( $p < 0.05$ ).

		$\theta$ (°C)	Salinity	$\sigma_\theta$ (kg m <sup>-3</sup> )	NO <sub>3</sub> <sup>-</sup> (μmol L <sup>-1</sup> )	DIC (μmol L <sup>-1</sup> )	Chl <i>a</i> (μg L <sup>-1</sup> )	POC (μmol L <sup>-1</sup> )	O <sub>2</sub> saturation (%)
Central Channel	WW	<b>-1.68 ± 0.04</b>	<b>32.88 ± 0.16</b>	<b>26.46 ± 0.13</b>	<b>12.0 ± 1.71</b>	<b>2203 ± 52</b>	3.53 ± 3.75	<b>18.7 ± 12.4</b>	<b>90.7 ± 6.8</b>
	Non-WW	1.00 ± 2.18	32.12 ± 0.73	25.70 ± 0.63	1.85 ± 3.15	2048 ± 101	5.40 ± 8.53	36.3 ± 33.1	114 ± 14.4
Chukchi North	WW	<b>-1.72 ± 0.05</b>	<b>32.88 ± 0.29</b>	<b>26.46 ± 0.24</b>	<b>12.1 ± 6.27</b>	<b>2225 ± 65</b>	<b>7.98 ± 9.56</b>	23.4 ± 17.0	<b>95.3 ± 10.9</b>
	Non-WW	0.61 ± 1.54	32.23 ± 0.57	25.83 ± 0.49	1.73 ± 3.76	2049 ± 96	2.35 ± 3.50	19.3 ± 14.2	112 ± 11.7
Chukchi Slope West	WW	<b>-1.71 ± 0.05</b>	<b>32.59 ± 0.42</b>	<b>26.23 ± 0.34</b>	<b>12.7 ± 6.21</b>	<b>2216 ± 77</b>	<b>9.18 ± 8.17</b>	19.7 ± 15.6	<b>97.9 ± 17.0</b>
	Non-WW	-0.14 ± 1.48	31.47 ± 0.88	25.25 ± 0.69	1.02 ± 2.57	2003 ± 76	5.33 ± 7.75	31.8 ± 25.6	117 ± 11.6
Hanna Shoal North	WW	<b>-1.72 ± 0.04</b>	<b>32.82 ± 0.26</b>	<b>26.41 ± 0.21</b>	<b>12.4 ± 5.56</b>	<b>2236 ± 48</b>	<b>10.4 ± 6.02</b>	<b>31.7 ± 12.6</b>	<b>93.8 ± 11.5</b>
	Non-WW	-0.43 ± 1.21	31.25 ± 0.99	25.09 ± 0.80	0.09 ± 0.19	1983 ± 77	1.66 ± 1.36	16.3 ± 6.2	119 ± 8.9
Chukchi Slope Center	WW	<b>-1.70 ± 0.03</b>	<b>32.39 ± 0.21</b>	<b>26.07 ± 0.17</b>	<b>13.7 ± 3.61</b>	<b>2252 ± 16</b>	<b>14.2 ± 19.8</b>	<b>44.9 ± 55.1</b>	<b>88.2 ± 12.6</b>
	Non-WW	-1.11 ± 0.70	29.77 ± 1.47	23.93 ± 1.19	0.51 ± 1.50	1996 ± 81	0.61 ± 1.58	5.7 ± 7.3	107 ± 7.0
Chukchi Slope East	WW	<b>-1.70 ± 0.04</b>	<b>32.41 ± 0.21</b>	<b>26.08 ± 0.17</b>	<b>12.5 ± 3.52</b>	<b>2236 ± 36</b>	<b>10.8 ± 9.51</b>	<b>39.4 ± 29.8</b>	<b>89.7 ± 13.5</b>
	Non-WW	-0.82 ± 0.79	30.38 ± 1.58	24.41 ± 1.3	0.90 ± 2.39	1983 ± 159	3.35 ± 6.55	10.3 ± 8.3	108 ± 8.6
Hanna Shoal Southeast	WW	<b>-1.64 ± 0.03</b>	<b>32.39 ± 0.19</b>	<b>25.98 ± 0.15</b>	<b>9.78 ± 4.45</b>	<b>2230 ± 45</b>	4.60 ± 4.04	17.6 ± 22.9	<b>85.6 ± 8.2</b>
	Non-WW	0.23 ± 1.63	31.16 ± 0.79	24.99 ± 0.68	1.22 ± 2.74	2056 ± 90	3.35 ± 6.55	14.1 ± 10.8	105 ± 7.9
All Transects	WW	<b>-1.71 ± 0.05</b>	<b>32.68 ± 0.37</b>	<b>26.30 ± 0.30</b>	<b>12.3 ± 5.13</b>	<b>2222 ± 63</b>	<b>8.64 ± 9.75</b>	<b>25.0 ± 22.5</b>	<b>94.1 ± 13.8</b>
	Non-WW	-0.21 ± 1.55	31.00 ± 1.49	24.87 ± 1.19	1.13 ± 2.71	2019 ± 107	2.79 ± 5.58	19.2 ± 21.4	110 ± 11.0

biological uptake in the upper 20 m of the water column.

There were three distinct areas of elevated phytoplankton biomass in the Central Channel transect (Fig. 3E and F), each in close proximity to a respective WW pathway. The large phytoplankton bloom associated with the northward flowing Central Channel WW pathway (St. 38–43) had the highest biomass, with

Chl *a* (Fig. 3E) and POC (Fig. 3F) concentrations of 16–30  $\mu\text{g L}^{-1}$  and 70–100  $\mu\text{mol L}^{-1}$ , respectively, that extended from the surface down to the interface between WW and non-WW at 13–20 m depth. Biomass was also elevated at the interface of the southward flowing WW pathway at 25 m depth (15.3  $\mu\text{g Chl } a \text{ L}^{-1}$  at St. 48) and immediately inshore of the WW in the Alaskan Coastal

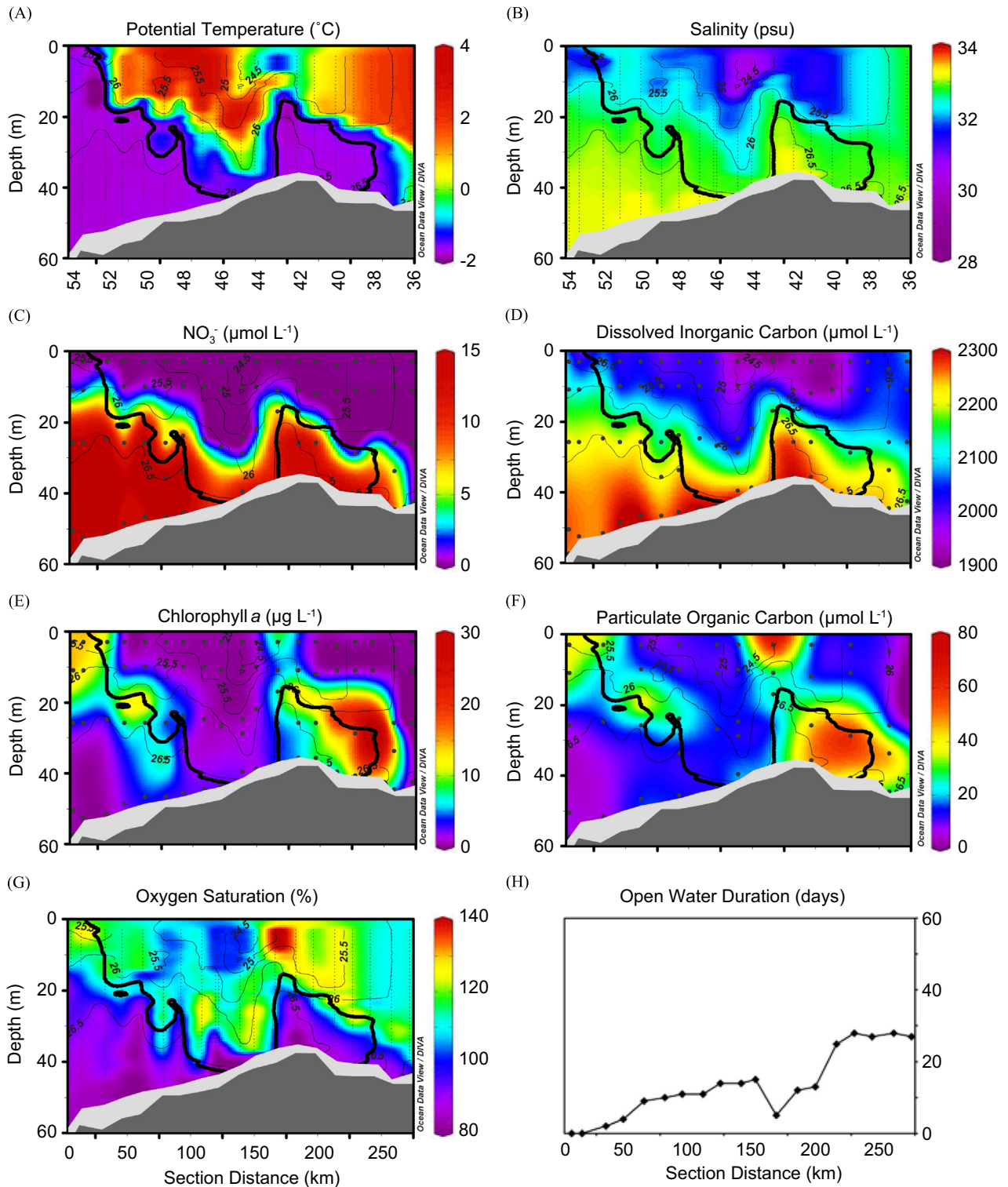


**Fig. 4.** The Chukchi North transect was sampled on 3–5 July 2011 and is displayed here from northwest (left) to southeast (right). (A–G) Hydrographic sections of (A)  $\theta$ , (B) salinity, (C)  $\text{NO}_3^-$ , (D) DIC, (E) Chl *a*, (F) POC, and (G)  $\text{O}_2$  saturation, overlain by  $\sigma_{\theta}$  ( $\text{kg m}^{-3}$ ; thin black lines with labels) and the WW isotherm ( $\theta = -1.6^{\circ}\text{C}$ ; thick black line). Station numbers are below (A) and (B) and black dots represent sampling depths. (H) Satellite-based open water duration, indicating the number of days each station was in open water from the time of ice retreat until the date of sampling. Note that because this transect was sampled in a different year than the Central Channel transect (Fig. 3), there are overlapping station numbers between the two transects that refer to different locations.

Current at 32 m depth ( $8.80 \mu\text{g Chl } a \text{ L}^{-1}$  at St. 53). The lowest concentrations of phytoplankton (e.g.  $< 1 \mu\text{g Chl } a \text{ L}^{-1}$ ; Fig. 3E) were found in surface waters that were depleted in nutrients (e.g. upper 15–20 m; St. 44–55) and in the light-limited WW (at 25–50 m depth) shaded by the large phytoplankton bloom in St. 38–43. WW in the Central Channel transect had lower phytoplankton biomass than non-WW (Table 1), based on POC concentrations of  $18.7 \pm 12.4 \mu\text{mol L}^{-1}$  and  $36.3 \pm 33.1 \mu\text{mol L}^{-1}$ , respectively ( $p=0.02$ ). Mean concentrations of Chl *a* for WW and non-WW were  $3.53 \pm 3.75 \mu\text{g L}^{-1}$  and  $5.40 \pm 8.53 \mu\text{g L}^{-1}$ , respectively, although these values did not represent a statistically significant difference. We note that the large phytoplankton bloom above the WW in the Central Channel pathway (St. 38–43) greatly influenced the non-WW means of this transect.

The  $\text{O}_2$  saturation (Fig. 3G) was highest (140–175%) within the large phytoplankton bloom (St. 38–45). Despite the low biomass in the surface waters east of this bloom (St. 44–55), the upper water column was supersaturated ( $> 100\%$ ) with  $\text{O}_2$ , indicative of recent photosynthesis throughout the transect. The observations of low POC and Chl *a* in the upper water column paired with high  $\text{O}_2$  saturation indicate that photosynthesis was likely followed by the sinking of phytoplankton cells to deeper in the water column, resulting in the higher biomass within WW at these stations. Across the Central Channel transect, the mean  $\text{O}_2$  saturation was higher in non-WW ( $114 \pm 14.4\%$ ) than in WW ( $90.7 \pm 6.8\%$ ) ( $p < 0.001$ ), revealing a pattern of supersaturation in the non-WW and undersaturation in WW. This pattern was consistent for all of the transects in this study (Table 1).

The satellite-derived open water duration (defined earlier in Section 2.5) reveals that there was large variation in the timing of ice retreat, with open water duration increasing markedly from west to east across the Central Channel transect (Fig. 3H). Waters where the large upper water column phytoplankton bloom was located (St. 38–43) were recently ice-covered (e.g. only one day of open water at St. 38 where Chl *a* concentrations were  $16\text{--}25 \mu\text{g L}^{-1}$ ); by contrast, waters with deeper and lower biomass (St. 44–55) had been open for much longer (e.g. 42 days at St. 48 and 50 days at St. 53).

### 3.2.2. Chukchi North

Located north of the Central Channel transect, the Chukchi North transect extended northwest to southeast across the Chukchi shelf (from left to right; Figs. 1, 2B, and 4) and was characterized by WW in two distinct locations (Fig. 4A). The larger of the two WW pathways was flowing poleward at speeds ranging from  $10\text{--}20 \text{ cm s}^{-1}$ . This is the northward extension of the Central Channel pathway with a contribution from the western-most pathway that has been diverted eastward from Herald Canyon, due to the topography of the shelf (Pickart et al., 2010; submitted for publication; Fig. 1). The smaller WW pathway was progressing southward from the northern Chukchi shelf at a slower speed ( $\leq 5 \text{ cm s}^{-1}$ ) (Figs. 1, 2B, and 4A).

The salinity range of WW in this transect (31.63–33.25) was greater than that of the Central Channel transect, due primarily to the lower salinity WW near the surface in the northwestern stations (54–53) where WW was present throughout the entire water column (Fig. 4B). The Chukchi North WW was colder than that of the previous transect ( $p < 0.001$ ), with a mean  $\theta$  of  $-1.72 \pm 0.05 \text{ }^\circ\text{C}$  (Table 1).

Concentrations of  $\text{NO}_3^-$  (Fig. 4C), silicate (not shown), phosphate (not shown), and DIC (Fig. 4D) were related to the distribution of WW, with the depth of the nutricline and the largest DIC gradient mirroring the vertical extent of WW in each of the two pathways.  $\text{NO}_3^-$  concentrations in this transect were seven-fold higher in WW than in non-WW ( $p < 0.001$ ), with mean values of  $12.1 \pm 6.27 \mu\text{mol L}^{-1}$  and  $1.73 \pm 3.76 \mu\text{mol L}^{-1}$ ,

respectively (Table 1). The northwestern stations where WW extended to the surface (St. 54–53) displayed the greatest variation in WW nutrients and DIC, with concentrations ranging from  $\sim 0 \mu\text{mol NO}_3^- \text{ L}^{-1}$  and  $2010 \mu\text{mol DIC L}^{-1}$  at the surface to  $19.7 \mu\text{mol NO}_3^- \text{ L}^{-1}$  and  $2270 \mu\text{mol DIC L}^{-1}$  at depth.

Concentrations of Chl *a* (Fig. 4E) and POC (Fig. 4F) showed two distinct phytoplankton blooms associated with the two WW pathways, with bloom depth related to the vertical extent of WW. For example, at stations where WW was present near the surface (St. 54–53; 43–42), the Chl *a* and POC maxima were near the surface. As the WW isotherm deepened towards the seafloor (e.g. St. 49–48; 40–38), the depth of maximum biomass also deepened. Note that the apparent discrepancy between Chl *a* and POC data at St. 49 (at  $\sim 35 \text{ m}$  depth) in Fig. 4 is an artifact of the absence of POC data at that station. Unlike the Central Channel transect where the highest biomass was located primarily above the WW, blooms along the Chukchi North transect had high biomass ( $10\text{--}50 \mu\text{g Chl } a \text{ L}^{-1}$ ) both at the interface with and within the WW, resulting in a mean Chl *a* concentration that was 3.4 times higher ( $p < 0.001$ ) in WW than in non-WW ( $7.98 \pm 9.56 \mu\text{g L}^{-1}$  and  $2.35 \pm 3.50 \mu\text{g L}^{-1}$ , respectively; Table 1). Phytoplankton abundances were low ( $< 1 \mu\text{g Chl } a \text{ L}^{-1}$  and  $< 15 \mu\text{mol POC L}^{-1}$ ) throughout the water column where WW was not present (St. 47–44), in  $\text{NO}_3^-$ -depleted non-WW above the subsurface blooms, and in the light-limited WW beneath the near-surface bloom in the northwest (St. 54–52).

Similar to the previous transect, the upper water column was supersaturated in  $\text{O}_2$ , with higher  $\text{O}_2$  saturation (maximum: 144%) between the surface and the WW isotherm (Fig. 4G).  $\text{O}_2$  was also supersaturated within WW near the sea surface (upper 15–20 m) at St. 54–53, in contrast to the previous transect where all WW was undersaturated in  $\text{O}_2$ . Even at stations where phytoplankton biomass was low and there was no WW,  $\text{O}_2$  was supersaturated (102–125%; St. 46–48) and nutrients were depleted except near the seafloor, signaling previous photosynthesis throughout the upper water column of all stations along the Chukchi North transect. Despite the high biomass contained within WW,  $\text{O}_2$  saturation was lower in WW than in non-WW ( $p < 0.001$ ), with mean values of  $95.3 \pm 10.9\%$  and  $112 \pm 11.7\%$ , respectively (Table 1).

Ice retreat across the Chukchi North transect (Fig. 4H) was characterized by two regions where open water duration increased from west to east: stations 54–44 (0–15 days) and stations 43–36 (5–31 days). Interestingly, both of these increases were correlated with the vertical extent of water column biogeochemical properties (Fig. 4A–G). In particular, the depth of maximum phytoplankton biomass, the WW isotherm, and the nitracline were shallowest at stations that were either still ice-covered or recently ice-free, and deepest at stations with longer open water duration. We note that the northwestern bloom (St. 54–48) comprised a portion of the massive under-ice phytoplankton bloom that extended 100 km farther into the fully consolidated ice pack, as described by Arrigo et al. (2012; 2014). The fact that the southeastern bloom (St. 43–36) displayed a similar relationship between biogeochemical properties and open water duration suggests that this bloom likely also developed underneath the ice (see Section 4.3 below).

### 3.2.3. Chukchi Slope West

The longest and most northern transect extended northwest to southeast from the upper continental slope ( $\sim 150 \text{ m}$  depth) across the Chukchi shelfbreak to the shallow water ( $\sim 40 \text{ m}$ ) northwest of Hanna Shoal (from left to right; Figs. 1, 2C and 5). WW was flowing weakly to the west ( $< 10 \text{ cm s}^{-1}$ ; Fig. 2C) at the northern end of the transect due to wind-driven upwelling that reversed the (normally eastward-flowing) shelfbreak jet (Spall et al., 2014). At the time of occupation of the section, the eastward flow of the jet was starting to become re-established at deeper levels in the water column. On the shelf, the circulation of WW

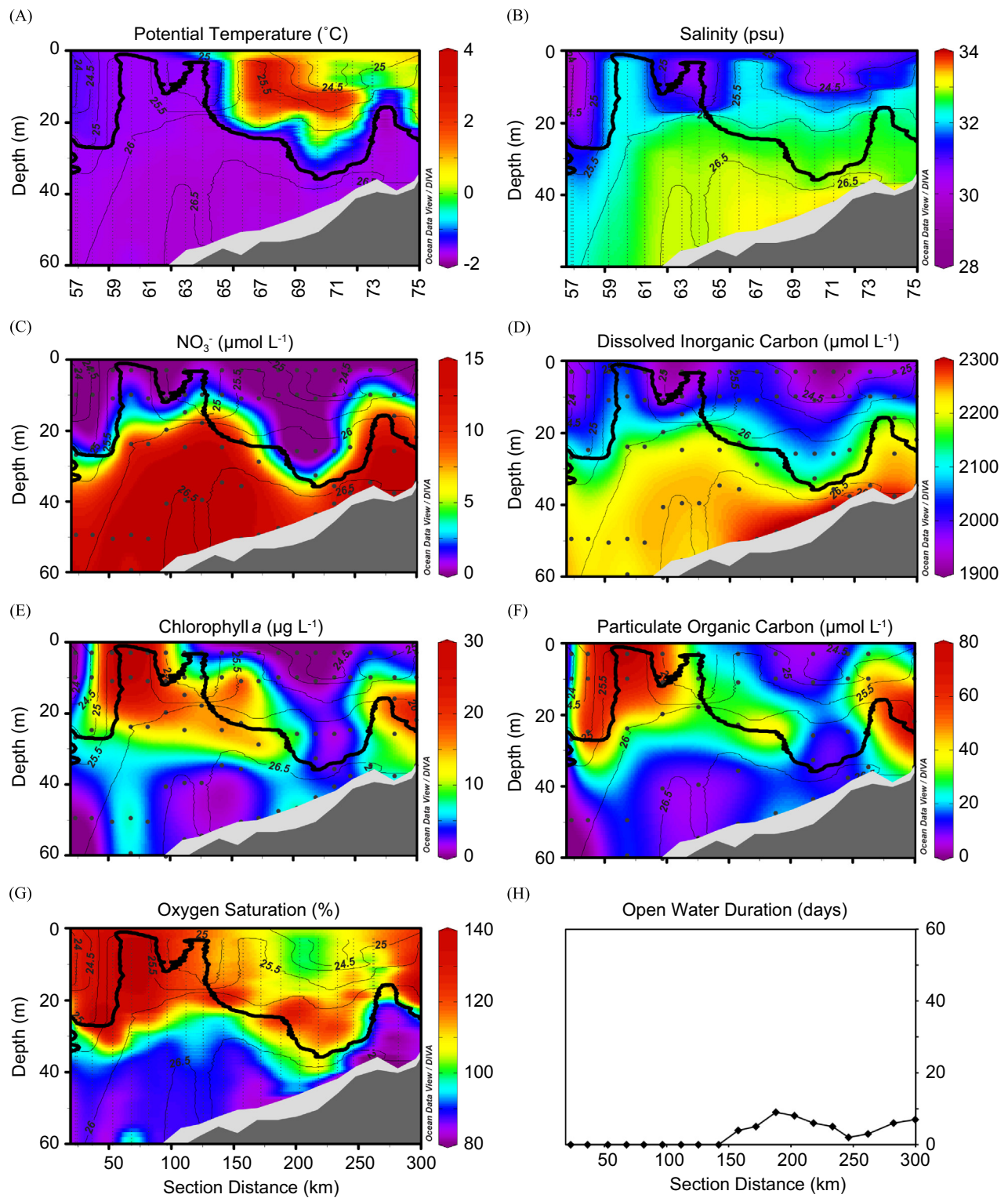


**Fig. 5.** The Chukchi Slope West transect was sampled from 7–9 July 2011 and is displayed here from northwest (left) to southeast (right). (A–G) Hydrographic sections of (A)  $\theta$ , (B) salinity, (C)  $\text{NO}_3^-$ , (D) DIC, (E) Chl *a*, (F) POC, and (G)  $\text{O}_2$  saturation, overlain by  $\sigma_{\theta}$  ( $\text{kg m}^{-3}$ ; thin black lines with labels) and the WW isotherm ( $\theta = -1.6^{\circ}\text{C}$ ; thick black line). Station numbers are below (A) and (B) and black dots represent sampling depths. (H) Satellite-based open water duration, indicating the number of days each station was in open water from the time of ice retreat until the date of sampling.

was the same as observed in the Chukchi North transect; i.e., northeastward flowing WW adjacent to equatorward-flowing WW closer to Hanna Shoal (compare Fig. 2B and C shoreward of the shelfbreak). Although restricted to the bottom 10 m at St. 70–72, WW was present at all stations along this  $\sim 300$  km long transect (Fig. 5A).

The Chukchi Slope West transect exhibited the widest range in WW salinity,  $\text{NO}_3^-$ , and DIC (Fig. 5B–D). Similar to previous transects, WW  $\text{NO}_3^-$  concentrations were high (mean:  $12.7 \pm 6.21 \mu\text{mol L}^{-1}$ ; Table 1) and the nitracline and the DIC gradient approximately mirrored the WW isotherm (Fig. 5C and D). The highest maximum  $\text{NO}_3^-$  concentrations on the shelf (upper 60 m) were measured

in this transect, with a maximum value of  $20.2 \mu\text{mol L}^{-1}$  in WW at St. 66. Surface waters were depleted in  $\text{NO}_3^-$  ( $\sim 0 \mu\text{mol L}^{-1}$ ), even where WW extended to the surface (St. 60–61).

A massive phytoplankton bloom was evident along the Chukchi Slope West transect, with Chl *a* and POC values of  $15\text{--}30 \mu\text{g L}^{-1}$  and  $50\text{--}100 \mu\text{mol L}^{-1}$ , respectively, throughout most of the upper 30–40 m of the water column (Fig. 5E and F). Biomass was lowest ( $< 0.5 \mu\text{g Chl } a \text{ L}^{-1}$ ) at stations where WW was at its minimum vertical extent (St. 68–72). Despite low light conditions caused by shading from the bloom above, concentrations of Chl *a* were relatively high in WW on the shelf beneath the massive phytoplankton bloom (St. 59–68; e.g. 40–60 m), with minimum Chl *a* concentrations of  $1\text{--}2 \mu\text{g L}^{-1}$  and some as high as  $5\text{--}10 \mu\text{g L}^{-1}$ . As with the previous transect, phytoplankton biomass was concentrated near the interface between WW and non-WW (Fig. 5E and F).

$\text{O}_2$  saturation was very high throughout the upper water column (Fig. 5G) in both WW and non-WW, with values as high as 130–150% between the surface and 25–30 m in the northwestern portion of the transect. At stations where the WW isotherm was deepest,  $\text{O}_2$  saturation was highest 10–20 m above the WW (St. 70–72). Similar to previous transects,  $\text{O}_2$  was undersaturated in bottom WW. However, due to the high levels of  $\text{O}_2$  produced in WW by the massive phytoplankton bloom at St. 57–69, this transect yielded the highest mean WW  $\text{O}_2$  saturation of all seven transects ( $p < 0.05$ ), with a mean of  $97.9 \pm 17.0\%$  (Table 1). Similarly, the  $\text{O}_2$  saturation in non-WW was also very high, with a mean of  $117 \pm 11.6\%$ .

The northwestern half of the Chukchi Slope West transect was still ice-covered at the time of sampling (Fig. 5H), with zero days of open water duration at St. 57–65 where the massive under-ice phytoplankton bloom was observed (Arrigo et al., 2012; 2014). Similar to the previous transect, there was a clear relationship between open water duration, the depth of the bloom, and the vertical extent of WW: both WW and the bloom reached the surface underneath the ice (St. 60–61) and extended deeper at stations with longer open water duration (e.g. St. 68–70, with 6–9 days open water duration, a WW isotherm depth of 25–39 m, and a biomass maximum of 35–45 m).

At three stations along the Chukchi Slope West transect, we also measured vertical profiles of the maximum efficiency of photosystem II (Fv:Fm) of phytoplankton (Fig. 6). Fv:Fm values were highest either at or slightly below the interface between WW and non-WW, where  $\text{NO}_3^-$  concentrations were high and light availability was sufficient for photosynthesis. In contrast, Fv:Fm values were lowest in the upper water column where light levels were high but nutrients were depleted ( $\sim 0 \mu\text{mol NO}_3^- \text{ L}^{-1}$ ), and in deeper waters where  $\text{NO}_3^-$  availability was high but light was limiting. For example, at St. 62 where WW was present in the

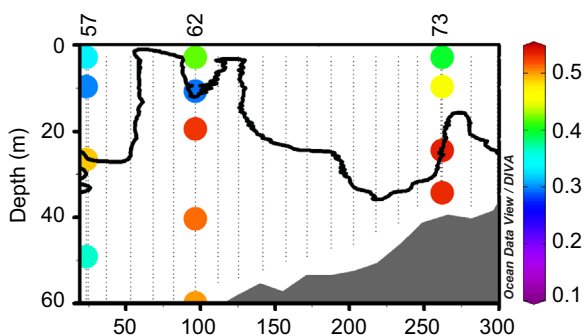


Fig. 6. Hydrographic section of Fv:Fm for three stations in the Chukchi Slope West transect. The section is overlain by the WW isotherm ( $\theta = -1.6 \text{ }^\circ\text{C}$ ; thick black line), consistent with biogeochemical properties displayed in Fig. 5A–G. Station numbers are listed above the plot.

upper water column, Fv:Fm was highest (0.53) several meters below the WW isotherm, reflecting the fact that phytoplankton growth had already depleted nutrients from shallower WW prior to our sampling.

### 3.2.4. Hanna Shoal North

Located east of the Chukchi Slope West transect, this section extended northwest to southeast from just beyond the shelf edge toward Hanna Shoal (from left to right; Figs. 1, 2D, and 7A). WW was observed at all stations. During our sampling period, the shelfbreak jet was fully re-established and advecting WW to east fairly rapidly ( $> 20 \text{ cm s}^{-1}$ ). Because of the relatively short distance between Hanna Shoal and the shelf edge, the eastward flowing pathway of WW on the outer shelf was not a distinct feature (as it was in the previous two transects), but instead was located immediately adjacent to the shelfbreak jet (Fig. 2D). In-shore of this, the WW returned southward next to Hanna Shoal as it had in the Chukchi Slope West section.

Phytoplankton biomass was high throughout the WW in this transect (Fig. 7E), with a mean Chl *a* concentration of  $10.4 \pm 6.02 \mu\text{g L}^{-1}$  (Table 1). By contrast, biomass was relatively low in the upper 20 m of the water column, with a mean non-WW Chl *a* concentration of  $1.66 \pm 1.36 \mu\text{g L}^{-1}$  (more than 6-fold lower than that of WW;  $p < 0.001$ ). We note that the apparent discrepancy between POC and Chl *a* concentrations results from a lack of POC data at St. 77 and St. 79 (Fig. 7E and F). Similar to previous transects, phytoplankton biomass was concentrated at the interface between WW and non-WW, with the highest Chl *a* concentrations just below the WW isotherm (Fig. 7E).

$\text{O}_2$  was supersaturated throughout the upper water column, with high  $\text{O}_2$  saturation extending from the surface to just below the WW isotherm (Fig. 7G). As with the previous transect,  $\text{O}_2$  saturation generally increased with depth towards the WW, with the highest values found just above the WW isotherm. Within WW,  $\text{O}_2$  saturation decreased with depth towards the seafloor. This transect exhibited the highest non-WW mean  $\text{O}_2$  saturation ( $119 \pm 8.9\%$ ; Table 1) of the study ( $p < 0.05$ ), signaling previous photosynthesis by phytoplankton despite the low biomass in non-WW relative to WW.

Most stations along this transect were sampled relatively soon after ice retreat (Fig. 7H). Only the southernmost station closest to Hanna Shoal had been open for more than a week prior to sampling (11 days; St. 82). This station also had the least amount of WW. Conversely, the northernmost stations (St. 76–77) were still ice covered at the time of sampling and had the greatest amount of WW. Between these two end points, the remaining stations (St. 78–81) had been open for 2–6 days prior to sampling and had a moderate amount of WW remaining on the shelf.

### 3.2.5. Chukchi Slope Center

Extending northeast to southwest from the base of the continental slope ( $\sim 2000 \text{ m}$ ) to the shallow waters ( $\sim 35 \text{ m}$ ) of Hanna Shoal, the Chukchi Slope Center transect was located east of the Hanna Shoal North transect (Fig. 1). WW was observed in the eastward-flowing shelfbreak jet, but not seaward of this. On the shelf, WW was once again being advected eastward in a distinct pathway, but the return flow was absent at this location since the transect was situated to the east of the bifurcation point of WW associated with Hanna Shoal (Fig. 1). As described by Pickart et al. (submitted for publication), the WW advected in the shelf pathway in this section was noticeably fresher than farther to the west (i.e. upstream), resulting in a lower mean WW salinity in this transect ( $32.39 \pm 0.21$ ) than in the previous transects (Table 1). Additionally, non-WW in this transect was the freshest and least dense of all seven transects (Table 1), with a mean salinity of  $29.77 \pm 1.47$  and a mean  $\sigma_\theta$  of  $23.93 \pm 1.19 \text{ kg m}^{-3}$  due in large part to the fresh and buoyant water sampled in the upper 20 m off

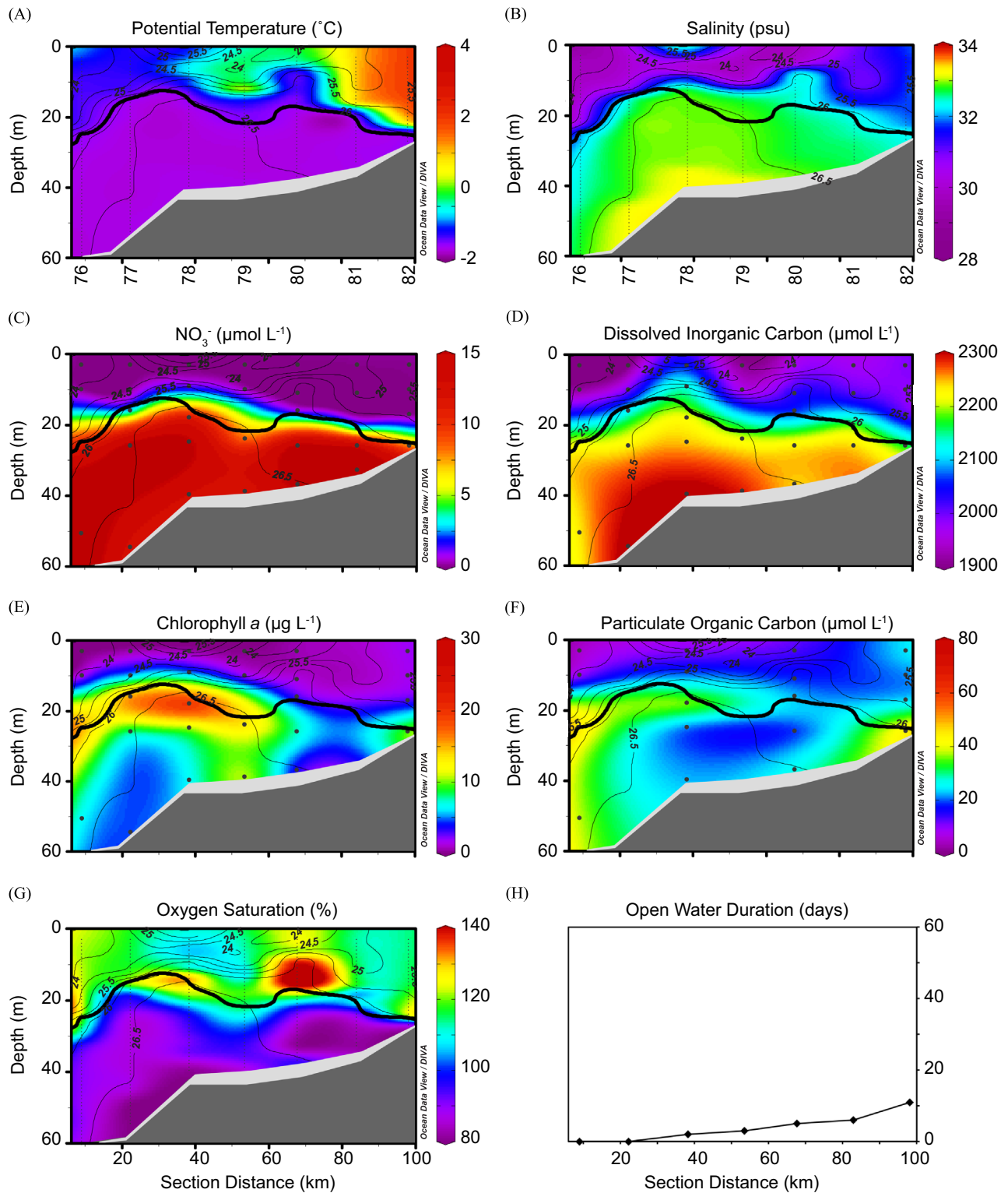


**Fig. 7.** The Hanna Shoal North transect was sampled on 9–10 July 2011 and is displayed here from northwest (left) to southeast (right). (A–G) Hydrographic sections of (A)  $\theta$ , (B) salinity, (C) NO<sub>3</sub><sup>-</sup>, (D) DIC, (E) Chl *a*, (F) POC, and (G) O<sub>2</sub> saturation, overlain by  $\sigma_\theta$  (kg m<sup>-3</sup>; thin black lines with labels) and the WW isotherm ( $\theta = -1.6$  °C; thick black line). Station numbers are below (A) and (B) and black dots represent sampling depths. (H) Satellite-based open water duration, indicating the number of days each station was in open water from the time of ice retreat until the date of sampling.

the shelf in the northeastern stations.

The maximum concentrations of NO<sub>3</sub><sup>-</sup> and DIC were associated with WW (Fig. 8C and D), although slightly elevated concentrations of NO<sub>3</sub><sup>-</sup> (~1 µmol L<sup>-1</sup>) and DIC (~2150 µmol L<sup>-1</sup>) were also found in non-WW at 40–60 m depth along the shelfbreak (St. 99–93) due to the upward tilt of the isopycnals progressing onshore.

This transect contained very high concentrations of WW NO<sub>3</sub><sup>-</sup> and DIC relative to the other transects, with means of  $13.7 \pm 3.61$  µmol L<sup>-1</sup> and  $2252 \pm 16$  µmol L<sup>-1</sup>, respectively (Table 1). The difference between mean NO<sub>3</sub><sup>-</sup> in WW and non-WW ( $0.51 \pm 1.50$  µmol L<sup>-1</sup>) was more than 25-fold ( $p < 0.001$ ), illustrating the extreme nutrient content of WW in relation to warmer

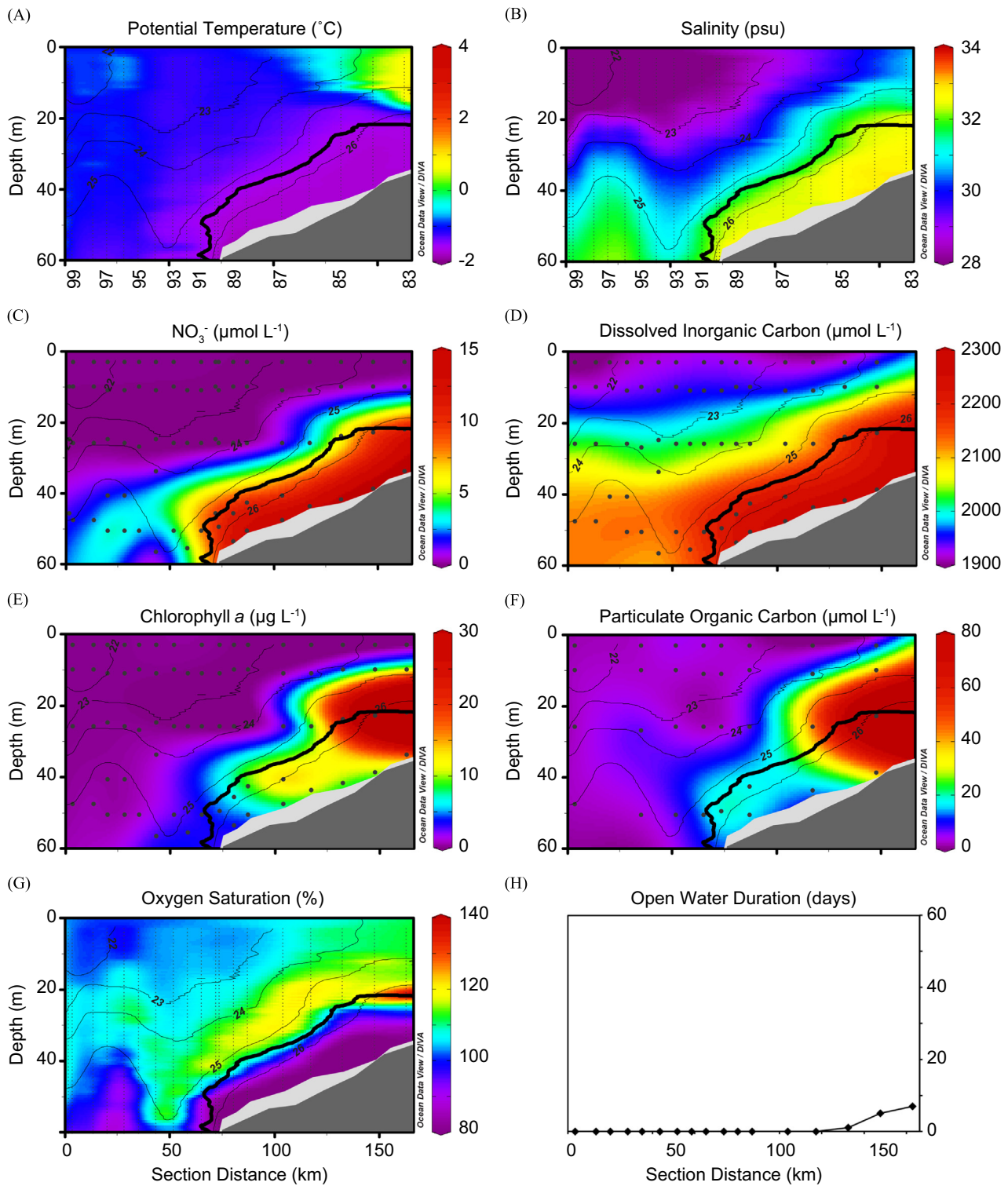


**Fig. 8.** The Chukchi Slope Center transect was sampled on 10–12 July 2011 and is displayed here from northeast (left) to southwest (right). (A–G) Hydrographic sections of (A)  $\theta$ , (B) salinity, (C)  $\text{NO}_3^-$ , (D) DIC, (E) Chl *a*, (F) POC, and (G)  $\text{O}_2$  saturation, overlain by  $\sigma_\theta$  ( $\text{kg m}^{-3}$ ; thin black lines with labels) and the WW isotherm ( $\theta = -1.6^\circ\text{C}$ ; thick black line). Station numbers are below (A) and (B) and black dots represent sampling depths. (H) Satellite-based open water duration, indicating the number of days each station was in open water from the time of ice retreat until the date of sampling.

waters on the Chukchi shelf.

Extremely high WW mean values of Chl *a* ( $14.2 \pm 19.8 \mu\text{g L}^{-1}$ ) and POC ( $44.9 \pm 55.1 \mu\text{mol L}^{-1}$ ) were observed on the Chukchi Slope Center transect (Table 1). These mean values were greatly influenced by an extremely large phytoplankton bloom at the interface between WW and non-WW (St. 85–83), with

maximum concentrations of Chl *a* ( $77.0 \mu\text{g L}^{-1}$  at St. 83) and POC ( $155 \mu\text{mol L}^{-1}$  at St. 84) that were the highest of the study (Fig. 8E and F). Conversely, biomass was very low in non-WW (except for 10–20 m above the WW isotherm), yielding non-WW mean values that were the lowest of the study ( $0.61 \pm 1.58 \mu\text{g Chl } a \text{ L}^{-1}$  and  $5.7 \pm 7.3 \mu\text{mol POC L}^{-1}$ ;  $p < 0.01$ ). The difference

between Chl *a* concentrations in WW and non-WW was 23-fold ( $p < 0.001$ ), resembling the difference in  $\text{NO}_3^-$  concentrations described above.

Open water duration was extremely short in this transect, with the majority of stations still under ice cover at the time of sampling

(zero days of open water duration at St. 99–86). The southwestern stations near Hanna Shoal (St. 85–83), where the massive phytoplankton bloom was located, were sampled in open water within 3–6 days of sea ice retreat. There were only 5–6 days of open water prior to sampling at St. 84–83, where the maximum phytoplankton

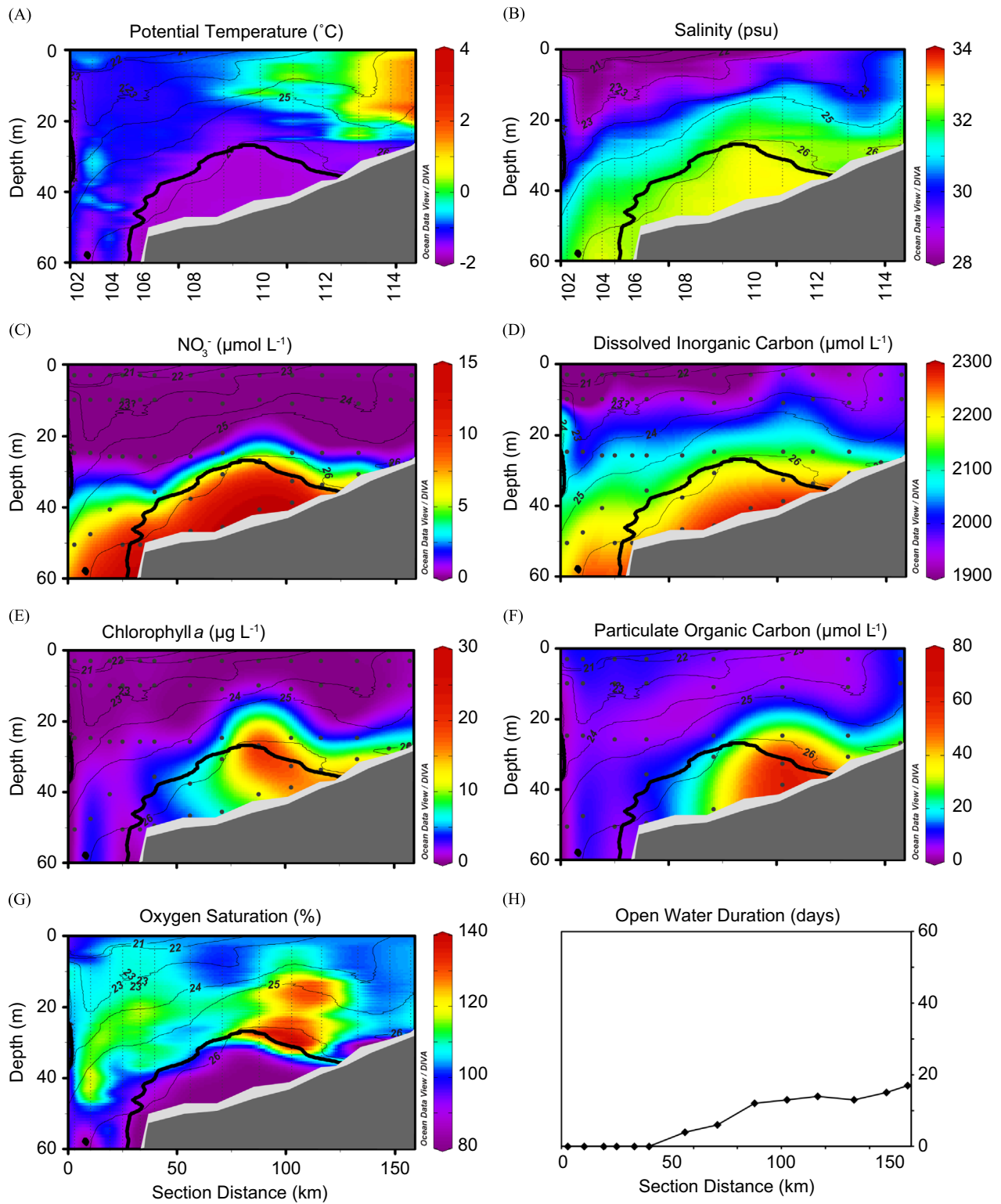


**Fig. 9.** The Chukchi Slope East transect was sampled on 14–16 July 2011 and is displayed here from northeast (left) to southwest (right). (A–G) Hydrographic sections of (A)  $\theta$ , (B) salinity, (C)  $\text{NO}_3^-$ , (D) DIC, (E) Chl *a*, (F) POC, and (G)  $\text{O}_2$  saturation, overlain by  $\sigma_\theta$  ( $\text{kg m}^{-3}$ ; thin black lines with labels) and the WW isotherm ( $\theta = -1.6^\circ\text{C}$ ; thick black line). Station numbers are below (A) and (B) and black dots represent sampling depths. (H) Satellite-based open water duration, indicating the number of days each station was in open water from the time of ice retreat until the date of sampling.

biomass was the highest of this study ( $73\text{--}77 \mu\text{g Chl } a \text{ L}^{-1}$ ).

### 3.2.6. Chukchi Slope East

Spanning the northeastern portion of the Chukchi Sea, the Chukchi Slope East transect extended northeast to southwest from the upper slope ( $\sim 350 \text{ m}$ ) to the shallow waters ( $\sim 25 \text{ m}$ ) of

Hanna Shoal (from left to right; Figs. 1, 2F, and 9). A single region of WW was located in the center of this transect within the bottom 15–20 m of the water column. The seaward portion of the WW was being advected by the shelfbreak jet, while the shoreward portion was contained in the shelf pathway advecting the cold water cyclonically around Hanna Shoal (Figs. 1 and 2F). The mean

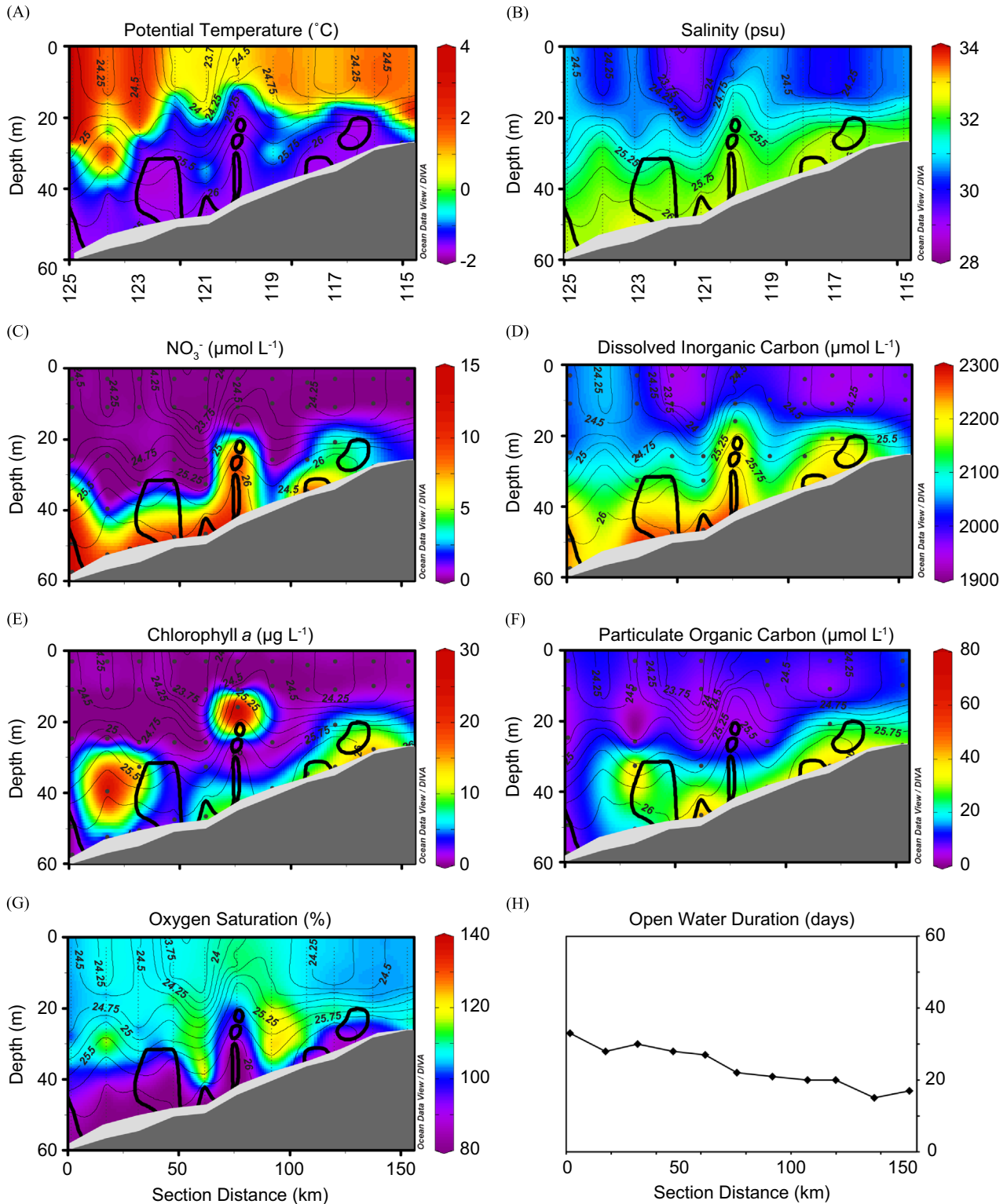


**Fig. 10.** The Hanna Shoal Southeast transect was sampled on 16 July 2011 and is displayed here from southeast (left) to northwest (right). (A–G) Hydrographic sections of (A)  $\theta$ , (B) salinity, (C)  $\text{NO}_3^-$ , (D) DIC, (E) Chl *a*, (F) POC, and (G)  $\text{O}_2$  saturation, overlain by  $\sigma_{\theta}$  ( $\text{kg m}^{-3}$ ; thin black lines with labels) and the WW isotherm ( $\theta = -1.6^{\circ}\text{C}$ ; thick black line). Station numbers are below (A) and (B) and black dots represent sampling depths. (H) Satellite-based open water duration, indicating the number of days each station was in open water from the time of ice retreat until the date of sampling.

$\theta$  ( $-1.70 \pm 0.04$  °C) and salinity ( $32.41 \pm 0.21$ ) of WW in the Chukchi Slope East transect was almost identical to that of the Chukchi Slope Center transect (Table 1), indicating that there was little modification of the WW as it progressed between the two transects. The range of non-WW salinity (19.74–32.49) was the largest here of all seven transects, with the freshest values at the surface near the shelfbreak (St. 106–108; Fig. 9B), indicating recent sea ice melt.

Consistent with previous transects,  $\text{NO}_3^-$  and DIC concentrations were extremely high within WW (Table 1), although relatively high concentrations were also found in the northeastern stations on the shelfbreak (St. 102–105) where WW was not present (Fig. 9C and D). Nutrients and DIC were depleted in non-WW in the upper 20–30 m of the water column ( $\sim 0$   $\mu\text{mol NO}_3^- \text{L}^{-1}$  and  $1950$   $\mu\text{mol DIC L}^{-1}$ ). The maximum  $\text{NO}_3^-$  concentration in this transect was  $18.5$   $\mu\text{mol L}^{-1}$ , the same as the maximum WW concentration along the Chukchi Slope Center transect.

There was a subsurface phytoplankton bloom associated with the nutrient-rich WW, illustrated by high concentrations of Chl *a* and POC (Fig. 9E and F). Biomass was most concentrated at the WW isotherm, with a maximum of  $30.6$   $\mu\text{g Chl } a \text{L}^{-1}$  at St. 110 where WW was at its shallowest extent (27 m depth). Biomass was relatively low at St. 106–107, where WW was confined to the light-limited waters below 40 m, and at St. 102–105 on the shelfbreak, where WW was not present. Mean Chl *a* and POC concentrations in WW were very high ( $10.8 \pm 9.51$   $\mu\text{g L}^{-1}$  and  $39.4 \pm 29.8$   $\mu\text{mol L}^{-1}$ , respectively; Table 1).

Stations at or near the shelfbreak were still ice-covered during our sampling period, with zero days of open water at St. 102–107. The remaining stations (St. 108–115) had been ice-free for 4–17 days, with open water duration increasing from northeast to southwest. The station with the highest biomass ( $> 30$   $\mu\text{g Chl } a \text{L}^{-1}$ ) and the largest extent of WW had been open for 12 days prior to sampling (St. 110), while stations closest to Hanna Shoal with no WW remaining on the shelf had been open for longer (15–17 days).

### 3.2.7. Hanna Shoal Southeast

The final section sampled along the anti-cyclonic WW pathway around Hanna Shoal was the Hanna Shoal Southeast transect, which extended southwest to northeast from the vicinity of Barrow Canyon towards Hanna Shoal (from left to right; Figs. 1, 2G, and 10). Although the outer shelf advection pathway was quite evident in this transect (Fig. 2G), only a small amount of WW was present within the pathway at the time of our sampling. This implies that the Hanna Shoal Southeast transect was near the leading edge of the WW at this point in the summer season, such that there was no WW downstream of this transect during our sampling period (as described in more detail in Pickart et al. (submitted for publication)). While the mean salinity of WW was similar to that of the previous two transects (Table 1), the mean  $\theta$  ( $-1.64 \pm 0.03$  °C) was the highest of all seven transects ( $p < 0.001$ ) and the density was the lowest ( $\sigma_\theta$ :  $25.98 \pm 0.15$   $\text{kg m}^{-3}$ ) ( $p < 0.001$ ). This transect contained only a small amount of WW rich in  $\text{NO}_3^-$  (Fig. 10C), with a relatively low mean of  $9.78 \pm 4.45$   $\mu\text{mol L}^{-1}$  (Table 1). Although still high, the maximum  $\text{NO}_3^-$  value ( $13.8$   $\mu\text{mol L}^{-1}$ ) was also the lowest maximum of all seven transects. In contrast, although DIC concentrations followed a similar pattern to  $\text{NO}_3^-$ , the mean WW DIC concentrations were not the lowest on the shelf (Table 1).

Phytoplankton abundance (Fig. 10E and F) was elevated at stations where WW was present and within remnant WW near the seafloor. There were two locations with very high phytoplankton biomass (St. 120 at 16 m and St. 124 at 40 m; both  $\sim 30$   $\mu\text{g Chl } a \text{L}^{-1}$ ). The bloom at St. 120 was concentrated at  $\sim 18$  m depth, where a small amount of WW provided a source

of  $\text{NO}_3^-$  in an otherwise nutrient-depleted section of the upper water column. The bloom at St. 124 was located at the northwestern boundary of the WW, although the highest biomass was contained in remnant WW at the time of sampling.

Consistent with the previous six transects,  $\text{O}_2$  saturation increased near the WW isotherm (Fig. 10G). However, the mean values of  $\text{O}_2$  saturation in both WW ( $85.6 \pm 8.2\%$ ) and non-WW ( $105 \pm 7.9\%$ ) were very low (Table 1), with the latter value representing the lowest non-WW mean of this study ( $p < 0.01$ ).

Every station in this transect had been ice-free for at least two weeks (Fig. 10H), with open water duration increasing from 17 days at St. 115 (near Hanna Shoal) to 33 days at St. 125 (closest to the Alaskan coast). The relatively long open water duration of this transect, paired with the relatively small amount of WW, depleted nutrients, and biomass mostly concentrated near the seafloor, indicated that we sampled this location after substantial primary production had already taken place. The only locations where phytoplankton continued to bloom were those that were influenced by a supply of nutrient-rich WW.

## 4. Discussion

### 4.1. Significance of nutrient-rich WW for phytoplankton blooms

The overarching theme that emerged in this study was that the presence of extremely cold WW ( $\theta \leq -1.6$  °C) was consistently associated with phytoplankton blooms. The relationship between phytoplankton and WW was driven not by temperature but by the extremely high nutrient content of this near-freezing water mass, particularly in the case of  $\text{NO}_3^-$ , which is the primary limiting nutrient in the Chukchi Sea (Cota et al., 1996; Codispoti et al., 2005; Tremblay et al., 2006). Plots of  $\theta$  versus  $\text{NO}_3^-$  for all water samples in the seven transects described above (Fig. 11A–G) illustrate that the highest concentrations of  $\text{NO}_3^-$  were found at extremely cold temperatures. Although slightly warmer remnant WW ( $-1.6$  °C  $< \theta < 0$  °C) occasionally contained relatively high nutrient concentrations, the vast majority of  $\text{NO}_3^-$  found on the Chukchi shelf was associated with WW ( $\theta \leq -1.6$  °C), with most concentrations between  $5$ – $20$   $\mu\text{mol L}^{-1}$ . Summer water masses ( $\theta > 0$  °C) contained virtually no  $\text{NO}_3^-$ , with concentrations frequently near  $0$   $\mu\text{mol L}^{-1}$  and always  $< 3.5$   $\mu\text{mol L}^{-1}$ . Across all seven transects, the mean  $\text{NO}_3^-$  concentration was more than 10-fold higher in WW than in warmer water ( $p < 0.001$ ), with a mean of  $12.3 \pm 5.13$   $\mu\text{mol L}^{-1}$  ( $n = 147$ ) for WW and  $1.13 \pm 2.71$  ( $n = 306$ ) for non-WW (Table 1). This relationship was consistent between years, as demonstrated by the two transects that were sampled in both 2011 and 2010: Chukchi North (Fig. 11B and H, respectively) and Hanna Shoal North (Fig. 11D and I, respectively). Concentrations of other dissolved nutrients were also very high in WW, although the relationship between water temperature and nutrient content was most consistent in the case of  $\text{NO}_3^-$ . The mean silicate concentration in WW ( $37.3 \pm 12.6$   $\mu\text{mol L}^{-1}$ ) was nearly five times higher than that of non-WW ( $7.53 \pm 7.89$   $\mu\text{mol L}^{-1}$ ) ( $p < 0.001$ ). Similarly, the mean phosphate concentration in WW ( $1.76 \pm 0.39$   $\mu\text{mol L}^{-1}$ ) was 2.4-fold greater than that of non-WW ( $0.73 \pm 0.31$   $\mu\text{mol L}^{-1}$ ) ( $p < 0.001$ ). Thus, as WW flows across the Chukchi shelf, it provides essential nutrients for phytoplankton that sustain primary production.

Driven by the high nutrient content of WW on the shelf, more phytoplankton biomass accumulated in this water mass than in warmer, nutrient-poor water (Table 1). Across all seven transects, the mean Chl *a* concentration was three-fold higher in WW ( $8.64 \pm 9.75$   $\mu\text{g L}^{-1}$ ;  $n = 133$ ) than in non-WW ( $2.79 \pm 5.58$   $\mu\text{g L}^{-1}$ ;  $n = 285$ ) ( $p < 0.001$ ). Concentrations of POC were  $\sim 25\%$  higher ( $p < 0.001$ ) in WW than in non-WW, with a mean of

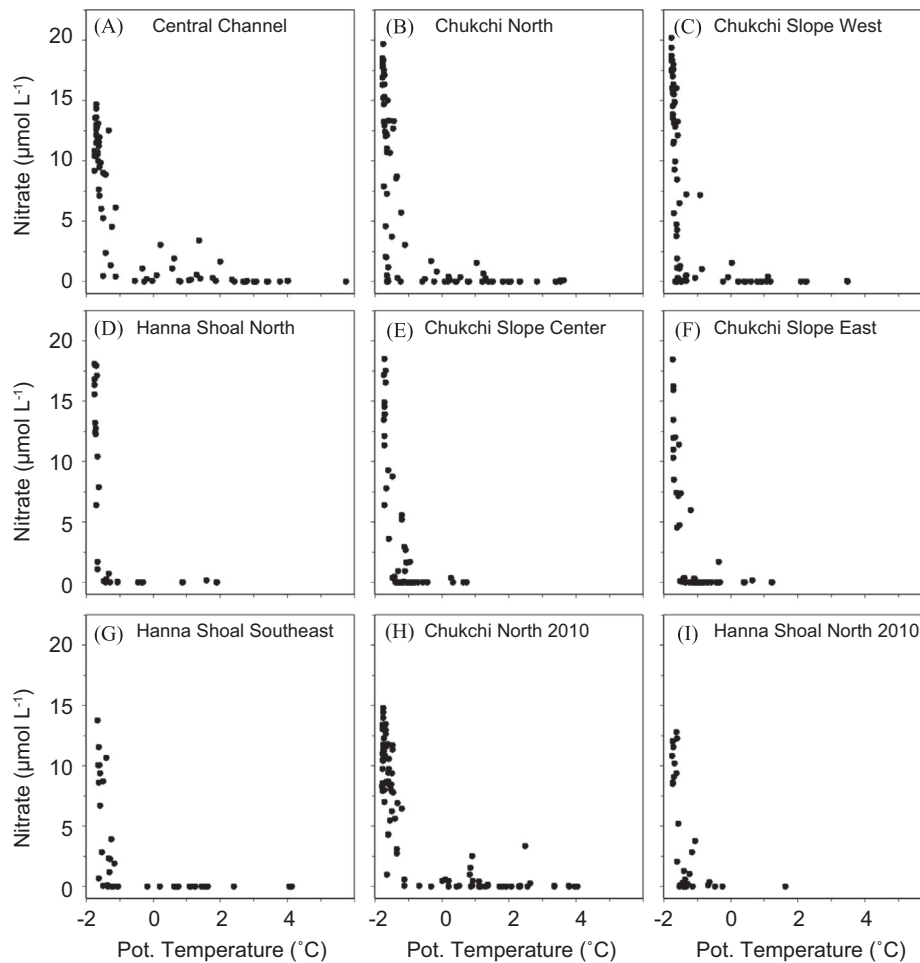


**Fig. 11.** Plots of potential temperature ( $\theta$ ) versus  $\text{NO}_3^-$  for all bottle samples in the upper 60 m from each transect: (A) Central Channel (2010), (B) Chukchi North, (C) Chukchi Slope West, (D) Hanna Shoal North, (E) Chukchi Slope Center, (F) Chukchi Slope East, (G) Hanna Shoal Southeast, (H) Chukchi North (2010), and (I) Hanna Shoal North (2010).

$25.0 \pm 22.5 \mu\text{mol L}^{-1}$  ( $n=76$ ) and  $19.2 \pm 21.4 \mu\text{mol L}^{-1}$  ( $n=164$ ), respectively. Similarly, although data are not shown for individual transects, the mean concentration of particulate organic nitrogen (PON) was  $\sim 40\%$  higher in WW ( $4.00 \pm 4.12 \mu\text{mol L}^{-1}$ ;  $n=75$ ) than in non-WW ( $2.67 \pm 2.71 \mu\text{mol L}^{-1}$ ;  $n=162$ ) ( $p < 0.001$ ). Phytoplankton physiology was also enhanced in nutrient-rich WW, with the mean maximum efficiency of photosystem II (Fv:Fm)  $\sim 24\%$  greater for phytoplankton sampled in WW ( $0.494 \pm 0.066$ ;  $n=6$ ) than for those in non-WW ( $0.389 \pm 0.080$ ;  $n=22$ ) ( $p=0.012$ ).

A second theme that emerged was that the vertical position of phytoplankton blooms in the water column was dictated by the vertical extent of WW, with maximum phytoplankton biomass concentrated at the interface between WW and non-WW (either at the same depth as or just above/below the WW isotherm, illustrated in Figs. 3–5 and 7–10). This pattern demonstrates the need of phytoplankton cells to balance nutrient availability with sufficient light for photosynthesis. Although  $\text{NO}_3^-$  concentrations were more than 10-fold higher in WW than adjacent non-WW, light availability was nearly 20-fold lower, with a mean PAR of  $5.99 \pm 44.9 \mu\text{Ein m}^{-2} \text{s}^{-1}$  in WW ( $n=1678$  one-meter light profile bins) compared to  $114 \pm 276 \mu\text{Ein m}^{-2} \text{s}^{-1}$  for non-WW ( $n=3155$ ) ( $p < 0.001$ ). Consequently, the interface between deeper, nutrient-rich WW and shallower, nutrient-poor water provided an balance between the competing needs of phytoplankton in the Chukchi Sea for  $\text{NO}_3^-$  and sunlight, leading to the presence of surface blooms at stations where WW was present in the upper water column and subsurface blooms at stations where the interface between WW

and non-WW was deeper. These results are consistent with previous work demonstrating maximum phytoplankton biomass at the nitracline in the Arctic (Tremblay et al., 2008; Martin et al., 2010; Ardyna et al., 2013), which, not surprisingly, was mostly at the same depth as the interface between WW and non-WW in our study. For a more detailed description of subsurface Chl *a* maxima (SCM) in the context of euphotic depth, the nitracline, and mixed layer depth in the Chukchi and Beaufort Seas, see Brown et al. (2015-b).

A third theme consistent across the seven transects in this study was that the upper water column was characterized by extremely high  $\text{O}_2$  content, with  $\text{O}_2$  saturation increasing towards the interface between WW and non-WW and decreasing within the WW interior (resulting in the characteristic supersaturation in non-WW and undersaturation in WW; Table 1). This feature illustrates that, prior to our sampling, photosynthesis took place primarily in the upper water column where light levels were optimal. By the time of our cruise, the supply of WW was largely confined to the lower part of the water column. Consequently, the deepened WW isotherm resulted in increased photosynthesis at greater depths and a sinking of phytoplankton cells from shallower depths where nutrients were depleted. This pattern resulted in frequent observations of extremely high phytoplankton biomass (e.g.  $30 \mu\text{g Chl } a \text{ L}^{-1}$ ) within WW, with very high  $\text{O}_2$  saturation (e.g. 140%) near the interface between WW and non-WW where cells were actively growing, and low  $\text{O}_2$  saturation (e.g. 80%) in deeper waters, where biomass likely accumulated primarily due to sinking processes. In these relatively deep waters, photosynthesis

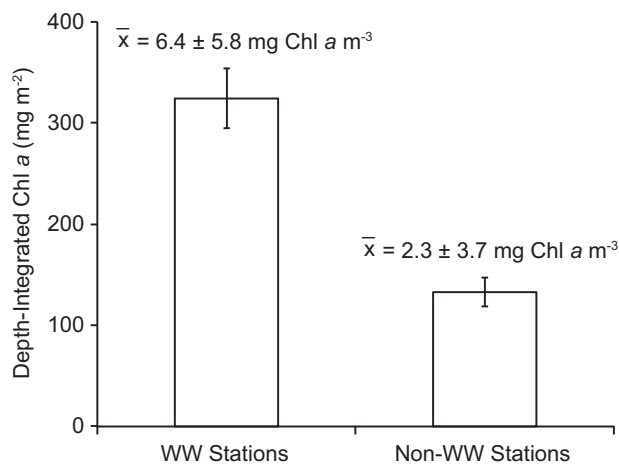


**Fig. 12.** Mean depth-integrated Chl *a* values with standard error bars for all winter water (WW) and non-winter water (non-WW) stations ( $n=100$  and  $n=202$ , respectively). Water column mean Chl *a* concentrations ( $\bar{x}$ ) and standard deviations ( $\pm$ SD) are also presented for WW and non-WW stations. Note that these values represent all ICESCAPE data collected in 2010 and 2011 and are not limited to shelf waters or the seven transects that we focus on in this study.

was limited by reduced light availability from self-shading by the bloom above and thus, O<sub>2</sub> production by phytoplankton was not sufficient to balance O<sub>2</sub> losses through respiration.

Finally, to assess whether the relationship between WW and phytoplankton blooms was widespread in this region, we compared Chl *a* concentrations to measurements of potential temperature at all stations and depths sampled during the ICESCAPE program in 2010 and 2011. This approach added an additional 198 stations to the seven transects presented here and extended the geographic range to include samples from the southern Chukchi Sea, Barrow Canyon, and the western Beaufort Sea (for locations of all ICESCAPE stations, see Arrigo et al. (2015)). Phytoplankton biomass was significantly higher at stations containing WW (at any depth in the water column) than at stations where WW was not present (Fig. 12), with depth-integrated Chl *a* concentrations that were 2.5-fold greater at WW stations ( $324 \pm 294$  mg m<sup>-2</sup>;  $n=100$ ) than at non-WW stations ( $133 \pm 205$  mg m<sup>-2</sup>;  $n=202$ ) ( $p < 0.001$ ). Similarly, mean Chl *a* concentrations throughout the water column were 2.8-fold greater at stations containing WW (Fig. 12;  $p < 0.001$ ). Thus, the presence of nutrient-rich WW was associated with higher phytoplankton biomass throughout the region across multiple years.

#### 4.2. Contribution of WW to biological hotspots

In this study, we sampled WW that was transported across the Chukchi shelf via a number of different pathways, including those that traveled through the Central Channel, from Herald Canyon, and along the Alaskan Coastal Current. These three main WW pathways branched out within the Chukchi Sea into smaller filaments, producing the complex pathway of WW flow illustrated in Fig. 1 and described in detail in Pickart et al. (submitted for publication). Many of these WW pathways ultimately converge in the northeastern Chukchi Sea, within the vicinity of the head of Barrow Canyon (Fig. 1). In fact, Barrow Canyon appears to be the primary outflow into the Arctic Basin for WW that flows across the Chukchi shelf (Pickart et al., 2005; Weingartner et al., 2005; Gong and Pickart, 2015). Notably, the region of WW confluence in the northeastern Chukchi Sea is characterized by extremely high rates of benthic production that support an abundance of benthic-feeding seabird and marine mammal populations (Dunton et al., 2005; Loeng et al., 2005; Grebmeier et al., 2006), leading to the

classification of this region as a macroinfaunal biomass 'hotspot' in the Pacific Arctic (Grebmeier et al., 2006; 2015).

We suggest that the exceptional productivity of the northeastern Chukchi Sea is driven in large part by the flow and confluence of multiple WW pathways in this region. Our study illustrates that nutrient-rich WW fuels primary production across the Chukchi shelf, resulting in phytoplankton blooms at all locations where WW intersected one of our seven transects. These findings indicate that photosynthesis occurs continuously along WW flow pathways on the shelf, leading to the accumulation of extremely high phytoplankton biomass within WW. Considering that water column grazing rates are relatively low in the Chukchi Sea (Campbell et al., 2009; Sherr et al., 2009), the high concentrations of phytoplankton contained in WW eventually sink to the seafloor. Consequently, the convergence of multiple highly productive WW pathways in the northeastern Chukchi Sea delivers a concentrated food source of sinking phytoplankton to the benthic community over an extended period of time. Thus, the flow of phytoplankton-abundant WW to the northeastern Chukchi Sea may play an essential and previously unrecognized role in sustaining the richness of this biological hotspot.

#### 4.3. Evidence for under-ice blooms

The massive phytoplankton bloom that we sampled underneath the ice in the northwestern portion of the Chukchi Slope West and Chukchi North transects (Figs. 4 and 5) was the first fully characterized under-ice bloom to be documented in the Chukchi Sea, as described previously (Arrigo et al., 2012, 2014). In the seven transects presented here, there was additional evidence of under-ice phytoplankton blooms at many stations that were either still ice covered or very recently ice-free at the time of sampling. For example, the Chukchi North transect contained an additional phytoplankton bloom with very high biomass (St. 43–37) located to the southeast of the previously documented massive under-ice bloom (St. 54–49; Fig. 4). The magnitude and vertical position of this phytoplankton bloom in relation to estimates of satellite-derived open water duration indicate similar mechanisms of bloom formation and progression as the nearby under-ice bloom. Thus, although sea ice had already retreated from the location of the southeastern bloom by the time we arrived, it is highly likely that this bloom also began beneath the ice, resulting in the measurements of elevated phytoplankton biomass at the surface in recently-ice free waters during our sampling period.

Comparing the magnitude of phytoplankton biomass in relation to open water duration at many additional stations also reveals evidence of under-ice blooms throughout the Chukchi Sea. For example, as described in Section 3.2.1, the large upper water column phytoplankton bloom in the Central Channel transect (Fig. 3) had very high biomass ( $16\text{--}25$   $\mu\text{g Chl } a \text{ L}^{-1}$  and  $70\text{--}85$   $\mu\text{mol POC L}^{-1}$ ) at St. 38, which we sampled on the day after sea ice retreat. Similarly, phytoplankton biomass was very high ( $15\text{--}23$   $\mu\text{g Chl } a \text{ L}^{-1}$ ) at the interface between WW and non-WW in St. 76–79 in the Hanna Shoal North transect (Fig. 7), where open water duration was 0–3 days. In the Chukchi Slope Center transect (Fig. 8), Chl *a* concentrations exceeded  $70$   $\mu\text{g L}^{-1}$  at St. 83 and 84, which had only been ice-free for 5–6 days. Across all seven transects comprising 105 stations, there were 21 stations with biomass  $> 20$   $\mu\text{g Chl } a \text{ L}^{-1}$ , with at least one station per transect. Open water duration at these stations was relatively short, with a mean of  $9.14 \pm 9.37$  days. Such high biomass in recently ice-free waters implies that phytoplankton at many of these stations must have begun to grow underneath the ice, considering that an initial Chl *a* concentration of  $0.02$   $\mu\text{g L}^{-1}$  at a relatively fast specific growth rate corresponding to a doubling per day ( $0.69 \text{ d}^{-1}$ ) would require two weeks to reach  $> 20$   $\mu\text{g Chl } a \text{ L}^{-1}$ .

Finally, O<sub>2</sub> saturation and nutrient concentrations indicate that

phytoplankton bloomed in all shelf waters across the seven transects prior to our sampling, regardless of open water duration.  $O_2$  was supersaturated throughout the upper water column, suggesting that widespread photosynthesis took place, even at stations that were still ice-covered or very recently ice free (e.g. in the Hanna Shoal North and Chukchi Slope Center transects). Similarly,  $NO_3^-$  and DIC concentrations were depleted throughout the upper water column, providing biogeochemical evidence of uptake by phytoplankton since the start of the growing season. Since open water duration was relatively short at many locations we sampled, these consistent signals of previous phytoplankton growth provide additional evidence that there were under-ice blooms throughout the study area prior to our sampling. The notion that under-ice blooms are prevalent in this region is consistent with the satellite-based estimate that  $>70\%$  of shelf waters in the Chukchi Sea support phytoplankton blooms underneath sea ice prior to ice retreat (Lowry et al., 2014).

#### 4.4. Conceptual model of phytoplankton blooms in the Chukchi Sea

The relationships between nutrient-rich WW, phytoplankton abundance, and open water duration identified in this study, combined with previous work, allows for the construction of a revised conceptual model of phytoplankton blooms in the Chukchi Sea.

In the winter, sea ice formation and brine rejection lead to convective overturning of the shallow water column on both the Chukchi and Bering Sea shelves (Muench et al., 1988; Weingartner et al., 1998; Woodgate et al., 2005b). This forms near-freezing WW and replenishes the surface ocean with high concentrations of nutrients that are mixed into the water column from the sediments. As the winter progresses, WW is advected into the Chukchi Sea through Bering Strait, and polynyas and smaller leads open up locally on the Chukchi shelf (Cavalieri and Martin, 1994; Iwamoto et al., 2014), which results in continued formation of WW. Hence, by the end of the winter, presumably the water column is fully mixed with nutrient-rich WW extending from the surface to the seafloor throughout much of the Chukchi shelf.

As sunlight returns to the ice-covered Chukchi Sea in the spring, solar heating begins to modify sea ice and the underlying water column. Melt ponds form on the surface of the ice (Polashenski et al., 2012), allowing sunlight to penetrate through the ice and into the water column. As warming continues, melt ponds expand on the relatively flat first-year sea ice that has become characteristic of the Chukchi Sea (Maslanik et al., 2011), increasing the availability of sunlight in the upper ocean. Previous work reveals that up to 55% of incident light is transmitted through first-year melt ponded ice (Frey et al., 2011). WW under the ice warms slightly from its extremely cold formation temperature near  $-1.9^\circ\text{C}$ , and also by mixing with more moderate waters entering through Bering Strait (Gong and Pickart, 2012). In our study, which took place in June/July, the mean observed WW temperature was  $-1.71 \pm 0.05^\circ\text{C}$ .

Once light availability under melt ponded ice is sufficient for primary production, phytoplankton blooms begin in surface waters beneath the ice on the Chukchi shelf (Arrigo et al., 2012, 2014, Palmer et al., 2014), fueled initially by the widespread presence of WW and subsequently by the continued input of WW from the Bering Sea. As phytoplankton blooms develop,  $O_2$  is produced through photosynthesis and nutrients and DIC are utilized for photosynthesis and cell growth. After  $NO_3^-$  is removed from surface waters, phytoplankton cells cease growing and begin to sink, while new cells grow deeper in the water column where nutrients are more abundant. This process continues as the blooms evolve, resulting in the vertical 'migration' of blooms from the surface to the depth of the nitracline (Brown et al., 2015-b). Although much of the phytoplankton biomass

observed in this study was located in open water and below the surface layer, the numerous observations of high  $O_2$  saturation and depleted  $NO_3^-$  and DIC concentrations throughout the upper water column (including at ice-covered stations) indicate that blooms begin earlier in surface waters throughout the Chukchi shelf, likely under sea ice and within nutrient-rich water.

As spring transitions to summer and sea ice begins to retreat from the Chukchi Sea, WW is increasingly modified through a combination of solar heating, mixing with summer water masses, and nutrient uptake by phytoplankton. At the same time, WW is flushed off the Chukchi shelf into the Canada Basin and replaced by summer water, so by mid-summer most of the WW is confined primarily to the advective pathways illustrated in Fig. 1. The residence time of nutrient-rich WW on the shelf depends largely on the flow speeds and length of the circulation pathways; as such, phytoplankton bloom duration is determined in large part by circulation in the Chukchi Sea. For example, based on hydrographic data collected in Barrow Canyon (Itoh et al., 2015), cold Pacific-origin water travels quickly along the coastal pathway in the Chukchi Sea via the Alaskan Coastal Current, which is consistent with previous studies (e.g. Weingartner et al., 1998). In contrast, the cold water drains for a longer period (hence more slowly) through the summer from the Central Channel pathway around the northern side of Hanna Shoal described here (Fig. 1). Pickart et al. (submitted for publication) compute an average advective speed of approximately  $12\text{ cm s}^{-1}$  along this pathway, implying a travel time of over three months for the water to progress from Bering Strait to the Hanna Shoal Southeast transect. Hence, this may explain the extended duration of open water phytoplankton blooms in the Chukchi Sea, which were the longest of any Arctic region from 1998–2009, with a mean of  $119 \pm 16.1$  days (Arrigo and Van Dijken, 2011).

Like its residence time, the vertical extent of WW varies spatially in the summer, extending to the surface at some locations and confined to deeper in the water column at others (with the interface between WW and non-WW approximating the depth of the nitracline). The presence and vertical position of phytoplankton were closely associated with the interface between WW and non-WW, where the nitracline provides a balance between nutrients and light. Conversely, the absence of WW on the shelf is accompanied by  $NO_3^-$  depletion, resulting in low phytoplankton biomass. Presumably, after WW completely flushes off of the Chukchi shelf in the late summer to early fall when waters are more stratified, phytoplankton concentrations are greatly reduced, with blooms occurring only when episodic mixing and/or storm events bring nutrients to the upper water column (e.g. Pickart et al., 2011; Ardyna et al., 2014).

A key aspect of this conceptual model is the flow of high-nutrient WW across the shelf that both initiates and sustains phytoplankton blooms in the Chukchi Sea. Given that WW forms locally on the shelf in polynyas and leads during the winter, this implies that blooms in surface waters under melt ponded sea ice are likely widespread across the Chukchi shelf in the spring and early summer. Our observations indicate, however, that phytoplankton blooms along the nutrient-rich WW pathways are extended for longer duration than in adjacent waters, with total bloom duration and the magnitude of primary production related to the residence time and vertical extent of WW flow. Considering that the timing of bloom initiation in the Arctic may be shifting to earlier in the season with a warming climate (Kahru et al., 2010; Arrigo et al., 2012), the role of WW in extending blooms may be particularly important to upper trophic level organisms that rely on the consumption of phytoplankton. Similarly, we have shown that WW flowing through the northeastern Chukchi Sea in the summer en route to Barrow Canyon is characterized by extremely high concentrations of phytoplankton cells that likely sink and

provide an important and continuous food source for the rich benthic community in this biological 'hotspot' region. This work furthers our understanding of the hydrographic controls on the timing, magnitude, and dynamics of phytoplankton blooms in the Chukchi Sea.

## Acknowledgments

This material is based upon work supported by the National Aeronautic and Space Administration under Grant no. NNX10AF42G and the National Science Foundation Graduate Research Fellowship under Grant no. DGE-0645962 to K.E. Lowry. The authors would like to acknowledge the scientists, captain, and crew of the USCGC Healy for their efforts during the HLY1001 and HLY1101 missions that supported the collection of field data. Additionally, we would like to thank Carolina Nobre for her efforts that improved the visualization of multiple figures presented in this manuscript.

## References

- Ardyna, M., Babin, M., Gosselin, M., Devred, E., B elanger, S., Matsuoka, A., Tremblay, J. .E., 2013. Parameterization of vertical chlorophyll *a* in the Arctic Ocean: impact of the subsurface chlorophyll maximum on regional, seasonal and annual primary production estimates. *Biogeosciences* 10, 4383–4404. <http://dx.doi.org/10.5194/bg-10-4383-2013>.
- Ardyna, M., Babin, M., Gosselin, M., Devred, E., Rainville, L., Tremblay, J.-E., 2014. Recent Arctic Ocean sea ice loss triggers novel fall phytoplankton blooms. *Geophys. Res. Lett.* 41, 6207–6212. <http://dx.doi.org/10.1002/2014GL061047>.
- Armstrong, F., Stearns, C.R., Strickland, J., 1967. The measurement of upwelling and subsequent biological process by means of the Technicon Autoanalyzer<sup>®</sup> and associated equipment. *Deep-Sea Res.* 14, 381–389. [http://dx.doi.org/10.1016/0011-7471\(67\)90082-4](http://dx.doi.org/10.1016/0011-7471(67)90082-4).
- Arrigo, K.R., 2015. Impacts of Climate on EcoSystems and Chemistry of the Arctic Pacific Environment (ICESCAPE). *Deep-Sea Res. II* 118 (PA), 1–6. <http://dx.doi.org/10.1016/j.dsr2.2015.06.007>.
- Arrigo, K.R., Perovich, D.K., Pickart, R.S., Brown, Z.W., van Dijken, G.L., Lowry, K.E., Mills, M.M., Palmer, M.A., Balch, W.M., Bates, N.R., Benitez-Nelson, C.R., Brownlee, E., Frey, K.E., Laney, S.R., Mathis, J., Matsuoka, A., Mitchell, B.G., Moore, G.W.K., Reynolds, R.A., Sosik, H.M., Swift, J.H., 2014. Phytoplankton blooms beneath the sea ice in the Chukchi Sea. *Deep-Sea Res.* 105, 1–16. <http://dx.doi.org/10.1016/j.dsr2.2014.03.018>.
- Arrigo, K.R., Perovich, D.K., Pickart, R.S., Brown, Z.W., Van Dijken, G.L., Lowry, K., Mills, M.M., Palmer, M.A., Balch, W.M., Bahr, F., Bates, N.R., Benitez-Nelson, C., Bowler, B., Brownlee, E., Ehn, J.K., Frey, K.E., Garley, R., Laney, S.R., Lubelczyk, L., Mathis, J., Matsuoka, A., Mitchell, B.G., Moore, G.W.K., Ortega-Retuerta, E., Pal, S., Polashenski, C.M., Reynolds, R.A., Schieber, B., Sosik, H.M., Stephens, M., Swift, J.H., 2012. Massive phytoplankton blooms under Arctic Sea ice. *Science* 336, 1408. <http://dx.doi.org/10.1126/science.1215065>.
- Arrigo, K.R., Van Dijken, G.L., 2011. Secular trends in Arctic Ocean net primary production. *J. Geophys. Res.* 116, C09011.
- Bates, N.R., Best, M.H.P., Hansell, D.A., 2005. Spatio-temporal distribution of dissolved inorganic carbon and net community production in the Chukchi and Beaufort Seas. *Deep-Sea Res. II* 52, 3303–3323.
- Bates, N.R., Cai, W.J., Mathis, J.T., 2011. The ocean carbon cycle in the western Arctic Ocean: distributions and air-sea fluxes of carbon dioxide. *Oceanography* 24, 186–201. <http://dx.doi.org/10.5670/oceanog.2011.71>.
- Brown, Z.W., Casciotti, K.L., Pickart, R.S., Swift, J.H., Arrigo, K.R., 2015-a. Aspects of the marine nitrogen cycle of the Chukchi Sea shelf and Canada Basin. *Deep-Sea Research II* 118 (PA), 73–87. <http://dx.doi.org/10.1016/j.dsr2.2015.02.009>.
- Brown, Z.W., Lowry, K.E., Palmer, M.A., Van Dijken, G.L., Mills, M.M., Pickart, R.S., Arrigo, K.R., 2015-b. Characterizing the subsurface chlorophyll *a* maximum in the Chukchi Sea. *Deep-Sea Research II* 118 (PA), 88–104. <http://dx.doi.org/10.1016/j.dsr2.2015.02.010>.
- Campbell, R.G., Sherr, E.B., Ashjian, C.J., Plourde, S., Sherr, B.F., Hill, V., Stockwell, D. A., 2009. Mesozooplankton prey preference and grazing impact in the western Arctic Ocean. *Deep-Sea Res. II* 56, 1274–1289. <http://dx.doi.org/10.1016/j.dsr2.2008.10.027>.
- Carmack, E., Wassmann, P., 2006. Food webs and physical–biological coupling on pan-Arctic shelves: unifying concepts and comprehensive perspectives. *Prog. Oceanogr.* 71, 446–477. <http://dx.doi.org/10.1016/j.pocean.2006.10.004>.
- Cavaliere, D.J., Martin, S., 1994. The contribution of Alaskan, Siberian, and Canadian coastal polynyas to the cold halocline layer of the Arctic Ocean. *J. Geophys. Res.* 99, 18343–18362. <http://dx.doi.org/10.1029/94JC01169>.
- Coachman, L.K., Aagaard, K., Tripp, R.B., 1975. *Bering Strait: The Regional Physical Oceanography*. University of Washington Press, Seattle, Washington.
- Codispoti, L.A., Flagg, C., Kelly, V., Swift, J.H., 2005. Hydrographic conditions during the 2002 SBI process experiments. *Deep-Sea Res. II* 52, 3199–3226.
- Codispoti, L.A., Kelly, V., Thessen, A., Matrai, P., Suttles, S., Hill, V., Steele, M., Light, B., 2013. Synthesis of primary production in the Arctic Ocean: III. Nitrate and phosphate based estimates of net community production. *Prog. Oceanogr.* 110, 126–150. <http://dx.doi.org/10.1016/j.pocean.2012.11.006>.
- Cooper, L.W., Whitledge, T.E., Grebmeier, J.M., Weingartner, T., 1997. The nutrient, salinity, and stable oxygen isotope composition of Bering and Chukchi Seas waters in and near the Bering Strait. *J. Geophys. Res.* 102, 12563–12573.
- Cota, G.F., Pomeroy, L.R., Harrison, W.G., Jones, E.P., Peters, F., Sheldon, W.M., Weingartner, T.R., 1996. Nutrients, primary production and microbial heterotrophy in the southeastern Chukchi Sea: Arctic summer nutrient depletion and heterotrophy. *Mar. Ecol. Prog. Ser.* 135, 247–258.
- Cullen, J.J., Davis, R.F., 2003. The blank can make a big difference in oceanographic measurements. *Limnol. Oceanogr. Bull.* 12, 29–35.
- Dunton, K.H., Goodall, J.L., Schonberg, S.V., Grebmeier, J.M., Maidment, D.R., 2005. Multi-decadal synthesis of benthic–pelagic coupling in the western arctic: role of cross-shelf advective processes. *Deep-Sea Res. II* 52, 3462–3477.
- Frey, K.E., Perovich, D.K., Light, B., 2011. The spatial distribution of solar radiation under a melting Arctic sea ice cover. *Geophys. Res. Lett.* 38, L22501.
- Gong, D., Pickart, R.S., 2012. Observations of circulation and water mass transformation in eastern Chukchi Sea. *Eos Trans. AGU*, abstract 10755. *Ocean Sciences Meeting 2012*.
- Gong, D., Pickart, R.S., 2015. Summertime Circulation in the Eastern Chukchi Sea. *Deep-Sea Research II* 118 (PA), 18–31. <http://dx.doi.org/10.1016/j.dsr2.2015.02.006>.
- Grebmeier, J.M., 2012. Shifting patterns of life in the Pacific Arctic and sub-Arctic Seas. *Annu. Rev. Mar. Sci.* 4, 63–78. <http://dx.doi.org/10.1146/annurev-marine-120710-100926>.
- Grebmeier, J.M., Bluhm, B.A., Cooper, L.W., Danielson, S., Arrigo, K.R., Blanchard, A.L., Clarke, J.T., Day, R.H., Frey, K.E., Gradinger, R.R., Kedra, M., Konar, B., Kuletz, K.J., Lee, S.H., Lovvorn, J.R., Norcross, B.L., Okkonen, S.R., Ecosystem characteristics and processes facilitating persistent macrobenthic biomass hotspots and associated benthivory in the Pacific Arctic, *Progress in Oceanography* (2015), doi: <http://dx.doi.org/10.1016/j.pocean.2015.05.006>.
- Grebmeier, J.M., Cooper, L.W., Feder, H.M., Sirenko, B.I., 2006. Ecosystem dynamics of the Pacific-influenced Northern Bering and Chukchi Seas in the Amerasian Arctic. *Prog. Oceanogr.* 71, 331–361. <http://dx.doi.org/10.1016/j.pocean.2006.10.001>.
- Hansell, D.A., Whitledge, T.E., Goering, J.J., 1993. Patterns of nitrate utilization and new production over the Bering–Chukchi shelf. *Cont. Shelf Res.* 13, 601–627.
- Holm-Hansen, O., Lorenzen, C.J., Holmes, R.W., Strickland, J.D.H., 1965. Fluorometric determination of Chlorophyll. *ICES J. Mar. Sci.* 30, 3–15. <http://dx.doi.org/10.1093/icesjms/30.1.3>.
- Itoh, M., Shimada, K., Kamoshida, T., McLaughlin, F., Carmack, E., Nishino, S., 2012. Interannual variability of Pacific winter water inflow through Barrow Canyon from 2000 to 2006. *J. Oceanogr.* 68, 575–592.
- Itoh, M., Pickart, R.S., Kikuchi, T., Fukamachi, Y., Ohshima, K.I., Simizu, D., Arrigo, K. R., Vagle, S., He, J., Ashjian, C.J., Mathis, J.T., Nishino, S., Nobre, C., 2015. Water properties, heat and volume fluxes of Pacific water in Barrow Canyon during summer 2010. *Deep-Sea Res.* 1102, 43–54. doi: <http://dx.doi.org/10.1016/j.dsr.2015.04.004>.
- Iwamoto, K., Ohshima, K.I., Tamura, T., 2014. Improved mapping of sea ice production in the Arctic Ocean using AMSR-E thin ice thickness algorithm. *J. Geophys. Res. Ocean.* 119, 3574–3594. <http://dx.doi.org/10.1002/2013JC009749>.
- Jakobsson, M., 2002. Hypsometry and volume of the Arctic Ocean and its constituent seas. *Geochim. Geophys. Geosyst.* 3, 1–18. <http://dx.doi.org/10.1029/2001GC000302>.
- Jakobsson, M., Grantz, A., Kristoffersen, Y., Macnab, R., 2004. The Arctic Ocean: boundary conditions and background information. In: Stein, R., Macdonald, R. W. (Eds.), *The Organic Carbon Cycle in the Arctic Ocean*. Springer, New York, pp. 1–5.
- Kahru, M., Brotas, V., Manzano-Sarabia, M., Mitchell, B.G., 2010. Are phytoplankton blooms occurring earlier in the Arctic? *Glob. Chang. Biol.* 17, 1733–1739. <http://dx.doi.org/10.1111/j.1365-2486.2010.02312.x>.
- Kolber, Z.S., Pr sil, O., Falkowski, P.G., 1998. Measurements of variable chlorophyll fluorescence using fast repetition rate techniques: defining methodology and experimental protocols. *Biochim. Biophys. Acta (BBA) – Bioenerg.* 1367, 88–106. [http://dx.doi.org/10.1016/S0005-2728\(98\)00135-2](http://dx.doi.org/10.1016/S0005-2728(98)00135-2).
- Kwok, R., Rothrock, D.A., 2009. Decline in Arctic sea ice thickness from submarine and ICESat records: 1958–2008. *Geophys. Res. Lett.* 36, L15501.
- Lee, S.H., Whitledge, T.E., Kang, S.-H., 2007. Recent carbon and nitrogen uptake rates of phytoplankton in Bering Strait and the Chukchi Sea. *Cont. Shelf Res.* 27, 2231–2249.
- Loeng, H., Brandt, K., Carmack, E., Denisenko, S., Drinkwater, K., Hansen, B., Kovacs, K., Livingston, P., McLaughlin, F., Sakshaug, E., 2005. *Marine Systems in: Arctic Climate Impact Assessment*. Cambridge University Press, Cambridge, UK, pp. 453–538.
- Lowry, K., Van Dijken, G.L., Arrigo, K.R., 2014. Evidence of under-ice phytoplankton blooms in the Chukchi Sea from 1998 to 2012. *Deep-Sea Res. II* 105, 105–117. <http://dx.doi.org/10.1016/j.dsr2.2014.03.013>.
- Martin, J., Tremblay, J. .E., Gagnon, J., Tremblay, G., Lapoussi re, A., Jose, C., Poulin, M., Gosselin, M., Gratton, Y., Michel, C., 2010. Prevalence, structure and properties of subsurface chlorophyll maxima in Canadian Arctic waters. *Mar. Ecol. Prog. Ser.* 412, 69–84. <http://dx.doi.org/10.3354/meps08666>.
- Maslanik, J., Stroeve, J., Fowler, C., Emery, W., 2011. Distribution and trends in Arctic sea ice age through spring 2011. *Geophys. Res. Lett.* 38, L13502.
- Mills, M.M., Brown, Z.W., Lowry, K., Van Dijken, G.L., Becker, S., Pal, S., Benitez-

- Nelson, C., Strong, A., Arrigo, K.R., 2015. Impacts of low phytoplankton  $\text{NO}_3^-$ :  $\text{PO}_4^{3-}$  utilization ratios over the Chukchi Shelf, Arctic Ocean. *Deep-Sea Research II* 118 (PA), 105–121. <http://dx.doi.org/10.1016/j.dsr2.2015.02.007>.
- Muench, R.D., Schumacher, J.D., Salo, S.A., 1988. Winter currents and hydrographic conditions on the northern central Bering Sea shelf. *J. Geophys. Res.* 93, 516–526. <http://dx.doi.org/10.1029/JC093iC01p00516>.
- Overland, J.E., Roach, A.T., 1987. Northward flow in the Bering and Chukchi Seas. *J. Geophys. Res.* 92, 7097–7105. <http://dx.doi.org/10.1029/JC092iC07p07097>.
- Padman, L. and S. Erofeeva, 2004: A barotropic inverse tidal model for the Arctic Ocean. *Geophys. Res. Lett.*, 31(2), L02303, doi:10.1029/2003GL019003.
- Palmer, M.A., Van Dijken, G.L., Greg Mitchell, B., Seegers, B.J., Lowry, K., Mills, M.M., Arrigo, K.R., 2013. Light and nutrient control of photosynthesis in natural phytoplankton populations from the Chukchi and Beaufort seas, Arctic Ocean. *Limnol. Oceanogr.* 58, 2185–2205. doi:10.4319/lo.2013.58.6.2185.
- Palmer, M.A., Saenz, B.T., Arrigo, K.R., 2014. Impacts of sea ice retreat, thinning, and melt-pond proliferation on the summer phytoplankton bloom in the Chukchi Sea, Arctic Ocean. *Deep-Sea Res. II* 105, 85–104.
- Pickart, R.S., Mao, C., and Bahr, F., submitted for publication. Winter water in the Chukchi Sea: a revised circulation scheme. *Deep-Sea Research II*.
- Pickart, R.S., Pratt, L.J., Torres, D.J., Whitedge, T.E., Proshutinsky, A.Y., Aagaard, K., Agnew, T.A., Moore, G., Dail, H.J., 2010. Evolution and dynamics of the flow through Herald Canyon in the western Chukchi Sea. *Deep-Sea Res. II* 57, 5–26.
- Pickart, R.S., Spall, M.A., Mathis, J.T., 2013. Dynamics of upwelling in the Alaskan Beaufort Sea and associated shelf–basin fluxes. *Deep-Sea Res. I* 76, 35–51.
- Pickart, R.S., Spall, M.A., Moore, G.W.K., Weingartner, T.J., Woodgate, R.A., Aagaard, K., Shimada, K., 2011. Upwelling in the Alaskan Beaufort Sea: atmospheric forcing and local versus non-local response. *Prog. Oceanogr.* 88, 78–100. <http://dx.doi.org/10.1016/j.pocean.2010.11.005>.
- Pickart, R.S., Weingartner, T.J., Pratt, L.J., Zimmermann, S., Torres, D.J., 2005. Flow of winter-transformed Pacific water into the Western Arctic. *Deep-Sea Res. II* 52, 3175–3198. <http://dx.doi.org/10.1016/j.dsr2.2005.10.009>.
- Polashenski, C.M., Perovich, D., Courville, Z., 2012. The mechanisms of sea ice melt pond formation and evolution. *J. Geophys. Res.* 117, C01001. <http://dx.doi.org/10.1029/2011JC007231>.
- Schlitzer, R., 2014. Ocean Data View. (<http://odv.awi.de>).
- Serreze, M.C., Holland, M.M., Stroeve, J., 2007. Perspectives on the Arctic's shrinking sea-ice cover. *Science* 315, 1533–1536.
- Sherr, E.B., Sherr, B.F., Hartz, A.J., 2009. Microzooplankton grazing impact in the Western Arctic Ocean. *Deep-Sea Res. II* 56, 1264–1273.
- Spall, M.A., Pickart, R.S., Brugler, E.T., Moore, G., Thomas, L., Arrigo, K.R., 2014. Role of shelfbreak upwelling in the formation of a massive under-ice bloom in the Chukchi Sea. *Deep-Sea Res. II* 105, 17–29. <http://dx.doi.org/10.1016/j.dsr2.2014.03.017>.
- Stroeve, J.C., Serreze, M.C., Holland, M.M., Kay, J.E., Malanik, J., Barrett, A.P., 2011. The Arctic's rapidly shrinking sea ice cover: a research synthesis. *Clim. Chang.* 110, 1005–1027. <http://dx.doi.org/10.1007/s10584-011-0101-1>.
- Tremblay, J.-E., Simpson, K., Martin, J., Miller, L., Gratton, Y., Barber, D.G., Price, N.M., 2008. Vertical stability and the annual dynamics of nutrients and chlorophyll fluorescence in the coastal, southeast Beaufort Sea. *J. Geophys. Res.* 113, C07S90. <http://dx.doi.org/10.1029/2007JC004547>.
- Tremblay, J.E., Michel, C., Hobson, K.A., Gosselin, M., Price, N.M., 2006. Bloom dynamics in early opening waters of the Arctic Ocean. *Limnol. Oceanogr.* 51, 900–912.
- Walsh, J.J., McRoy, C.P., Coachman, L.K., Goering, J.J., Nihoul, J.J., Whitedge, T.E., Blackburn, T.H., Parker, P.L., Wirick, C.D., Shuert, P.G., Grebmeier, J.M., Springer, A.M., Tripp, R.D., Hansell, D.A., Djenidi, S., Deleersnijder, E., Henriksen, K., Lund, B.A., Andersen, P., Mullerkarger, F.E., Dean, K., 1989. Carbon and nitrogen cycling within the Bering/Chukchi Seas – source regions for organic-matter affecting AOU demands of the Arctic Ocean. *Prog. Oceanogr.*, 22; , pp. 277–359.
- Weingartner, T., Aagaard, K., Woodgate, R., Danielson, S., Sasaki, Y., Cavalieri, D., 2005. Circulation on the north central Chukchi Sea shelf. *Deep-Sea Res. II* 52, 3150–3174.
- Weingartner, T.J., Cavalieri, D.J., Aagaard, K., Sasaki, Y., 1998. Circulation, dense water formation, and outflow on the northeast Chukchi shelf. *J. Geophys. Res.* 103, 7647–7661.
- Woodgate, R.A., Aagaard, K., 2005a. Monthly temperature, salinity, and transport variability of the Bering Strait through flow. *Geophys. Res. Lett.* 32, L04601. <http://dx.doi.org/10.1029/2004GL021880>.
- Woodgate, R.A., Aagaard, K., 2005b. Revising the Bering Strait freshwater flux into the Arctic Ocean. *Geophys. Res. Lett.* 32, L02602. <http://dx.doi.org/10.1029/2004GL021747>.
- Woodgate, R.A., Aagaard, K., Swift, J.H., Falkner, K.K., Smethie, W.M.J., 2005a. Pacific ventilation of the Arctic Ocean's lower halocline by upwelling and diapycnal mixing over the continental margin. *Geophys. Res. Lett.* 32, L18609. <http://dx.doi.org/10.1029/2005GL023999>.
- Woodgate, R.A., Aagaard, K., Weingartner, T.J., 2005b. A year in the physical oceanography of the Chukchi Sea: moored measurements from autumn 1990–1991. *Deep-Sea Res. II* 52, 3116–3149.
- Woodgate, R.A., Weingartner, T.J., Lindsay, R., 2012. Observed increases in Bering Strait oceanic fluxes from the Pacific to the Arctic from 2001 to 2011 and their impacts on the Arctic Ocean water column. *Geophys. Res. Lett.* 39, L24603. <http://dx.doi.org/10.1029/2012GL054092>.
- Zhang, J., Spitz, Y.H., Steele, M., Ashjian, C.J., Campbell, R., Berline, L., Matrai, P., 2010. Modeling the impact of declining sea ice on the Arctic marine planktonic ecosystem. *J. Geophys. Res.* 115, 1–24.